

Discretized Clay Shell Model (DCSM) of Clayey Sandstone: Evaluating the Effective Stress Coefficient of Permeability

Pin-Lun Tai¹ and Jia Jyun Dong¹

¹National Central University, Taiwan

November 23, 2022

Abstract

The effective stress coefficient determines the effective stress, which dominating the permeability of rocks. However, the documented value of for rocks shows a high scatter (0.3-5.5), based on the laboratory measurement. The well know Clay Shell Model (CSM) successfully explain why the of the clayey sandstone can well above 1 theoretically. However, CSM cannot account for the stress dependency of observed experimentally. In this study, a modification of CSM was proposed. This proposed Discretized Clay Shell Model (DCSM) discretizing multi-layers clay domain to account for the stress dependent elastic modulus of clay. Response surface method was used to determine the effective stress coefficient under different combination of confining stress and pore pressure. The parametric study and the prediction of permeability-depth relation using synthetic case illustrate the superior features of the proposed DCSM to the traditional CSM, especially when the clay content is high. Critical findings includes: (1) The predicted effective stress coefficient form a concaving upward surface in the pore pressure-confining stress space using DCSM even when the material properties of clay and grain remain unchanged. (2) The influence of pore pressure on (positive correlation) will be stronger than the influence of confining stress especially under low pore pressure. (3) The predicted is not necessary positively or negatively correlated to confining stress under constant pore pressure. (4) The predicted for soft, high stress dependent deformability of clay coating on the pores of sandstones could be far higher than 1.

Table S3. A synthetic case in this study

Burial depth (m)	Vertical Stress (MPa)	Pore pressure (MPa)	¹ α determined by ² DCSM	³ σ_{eff} (MPa) [$\alpha=0.6$]	⁴ k (m ²) [$\alpha=0.6$]	σ_{eff} (MPa) [α determined by DCSM]	k (m ²) [α determined by DCSM]
0	0	0		0.0	1.00E-15	0.00	1.00E-15
0.2	5	2	1.88	3.8	5.03E-16	1.25	7.98E-16
0.4	10	4	1.75	7.6	2.53E-16	2.99	5.82E-16
0.6	15	6	1.67	11.4	1.27E-16	4.95	4.08E-16
0.8	20	8	1.61	15.2	6.39E-17	7.09	2.77E-16
1	25	10	1.56	19.0	3.21E-17	9.35	1.84E-16
1.2	30	12	1.52	22.8	1.61E-17	11.72	1.20E-16
1.4	35	14	1.49	26.6	8.11E-18	14.15	7.72E-17
1.6	40	16	1.46	30.4	4.08E-18	16.63	4.93E-17
1.8	45	18	1.44	34.2	2.05E-18	19.16	3.12E-17
2	50	20	1.42	38.0	1.03E-18	21.68	1.97E-17

¹Effective stress coefficient denoted as α .

²Discretized Clay Shell Model (DCSM) proposed by this research.

³Effective stress denoted as σ_{eff} .

⁴Permeability denoted as k .

Table S1. Stress dependent shear modulus of Clay1, 2, and 3

Radial stress (MPa)	Shear modulus (GPa)	Shear modulus (GPa)	Shear modulus (GPa)
	[Clay1]	[Clay2]	[Clay3]
0	0.46	1.26	2.26
5	0.90	1.55	2.36
10	1.29	1.80	2.44
15	1.64	2.03	2.52
20	1.94	2.22	2.58
25	2.19	2.39	2.64
30	2.40	2.52	2.68
35	2.56	2.63	2.73
40	2.67	2.70	2.74
45	2.74	2.75	2.76
50	2.76	2.76	2.76

Supporting Information for

[Discretized Clay Shell Model (DCSM) of Clayey Sandstone: Evaluating the Effective Stress Coefficient of Permeability]

[P. L. Tai¹, J. J. Dong^{1,2}]

¹ Graduate Institute of Applied Geology, National Central University, Taoyuan 32001, Taiwan

² Earthquake-Disaster & Risk Evaluation and Management Center, National Central University, Taoyuan 32001, Taiwan]

Contents of this file

Table S1 to stress dependent shear modulus of Clay1, 2, and 3

Table S2 to all data of stress dependent effective stress coefficient

Table S3 to synthetic case in this research

Introduction

This supporting file shows all of data used in parameter analysis of this study. Table S1 supports the Fig. 8a in the main text. Table S2 supports the Fig. 11 in Section 4.4.1, Fig. 12 in Section 4.4.2, Fig. 13 in Section 4.4.3, and Fig. 15 in Section 5.1.3. Finally, Table S6 supports the synthetic case in Section 5.2.

21 for the stress dependency of α observed experimentally. In this study, a modification of CSM was
22 proposed. This proposed Discretized Clay Shell Model (DCSM) discretizing multi-layers clay
23 domain to account for the stress dependent elastic modulus of clay. Response surface method was
24 used to determine the effective stress coefficient α under different combination of confining stress
25 and pore pressure. The parametric study and the prediction of permeability-depth relation using
26 synthetic case illustrate the superior features of the proposed DCSM to the traditional CSM,
27 especially when the clay content is high. Critical findings includes: (1) The predicted effective stress
28 coefficient α form a concaving upward surface in the pore pressure-confining stress space using
29 DCSM even when the material properties of clay and grain remain unchanged. (2) The influence of
30 pore pressure on α (positive correlation) will be stronger than the influence of confining stress
31 especially under low pore pressure. (3) The predicted α is not necessary positively or negatively
32 correlated to confining stress under constant pore pressure. (4) The predicted α for soft, high stress
33 dependent deformability of clay coating on the pores of sandstones could be far higher than 1.

34

35 **1 Introduction**

36 The stress dependent permeability k of sandstone, one of the important reservoirs, is a key
37 parameter for fossil fuel exploitation (e.g., Li et al., 2008) and carbon geological sequestration (e.g.,
38 Cui et al., 2007). The general stress dependency of permeability k can be expressed as $k =$
39 $f(\sigma_c, P_p)$, where σ_c is confining stress and P_p is pore pressure. This two-variable function can be
40 replaced by a single variable function $k = f(\sigma_{eff})$ if an effective stress principle is valid (e.g.,

41 Bernabe, 1987; Al-Wardy and Zimmerman, 2004; Li et al., 2009; 2014), where σ_{eff} is the effective
 42 stress.

43 The effective stress dominating the permeability of rocks has been defined by many researchers
 44 (e.g., Bernabe, 1987; Berryman, 1992; Al-Wardy and Zimmerman, 2004; Li et al, 2009, 2014) as
 45 follows:

$$46 \quad \sigma_{eff} = \sigma_c - \alpha P_p \quad (1)$$

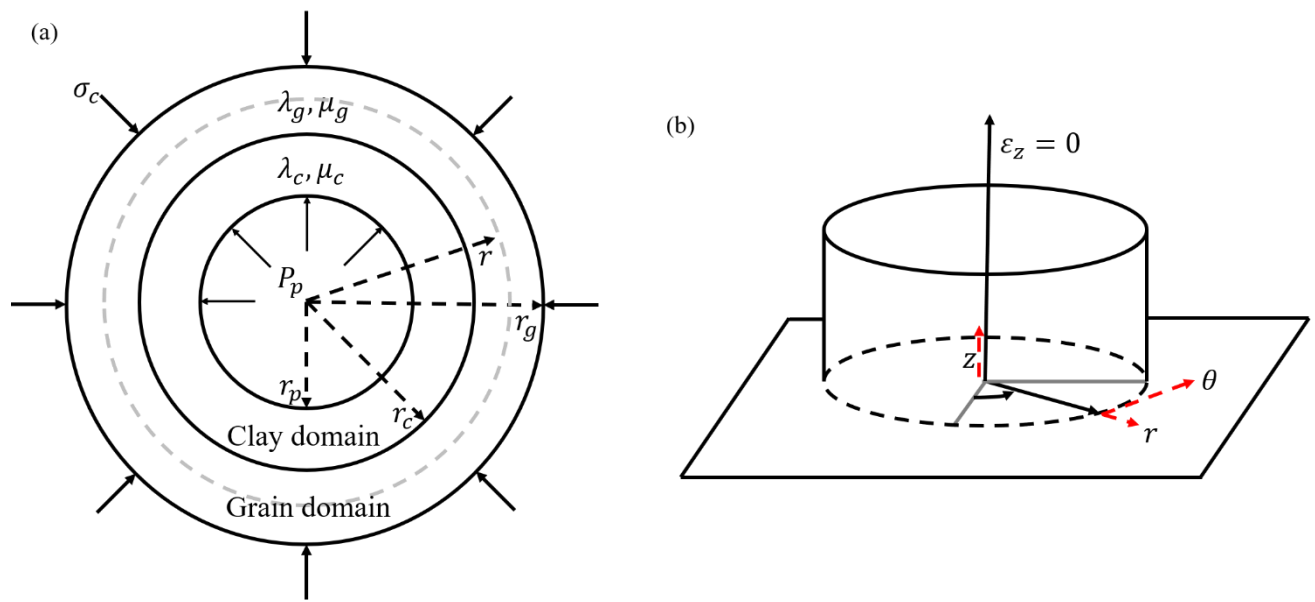
47 where α is effective stress coefficient of permeability. This parameter α is a measure of the
 48 relative sensitivity of pore pressure and confining pressure to the permeability k (Al-Wardy and
 49 Zimmerman, 2004). If α is a constant, the effective stress σ_{eff} can easily be determined by σ_c
 50 and P_p , separately.

51 When the confining stress are significantly larger than the pore pressure (e.g., permeability
 52 measurement in laboratory under high confining stress), precise determination of the effective stress
 53 coefficient α is not critical due to minor contribution of the P_p to effective stress when Eq. (1) was
 54 used. However, many sedimentary basins on continental margins hold abnormally high pore pressure
 55 at depths (Breckels, 1982; Gaarenstroom et al., 1993; Engelder and Fischer, 1994). The parameter α
 56 become critical for predicting the permeability k at burial depth. Moreover, the de-pressurization
 57 during the production lifecycle of a reservoir changes the pore pressure P_p and the effective stress
 58 σ_{eff} can only be evaluated if α can be determined in prior. Although different effective stress
 59 dependent relations of permeability are available (e.g., Dong et al., 2010), the prediction of
 60 sandstones' permeability at different depths are still challenge, since the comprehension of effective
 61 stress coefficient α at different burial depth is limited.

62 For most of the rocks (e.g., crystalline rocks, clean granular rocks, chalks, shales and so forth),
 63 the values of α close to but lower than 1 have been reported (e.g., Berryman, 1992). Some
 64 experimental studies found α of clayey sandstone and tight sandstone range in 0.60 to 0.85. (e.g.

65 Abass et al., 2009). However, Zoback and Byerlee (1975) measured permeability of the clayey Berea
 66 sandstone and found the α is ranging from 2.20 to 4.00. This result was supported by other
 67 experimental studies such as Walls and Nur (1979). To account for the observations of α larger than
 68 1, Zoback and Byerlee (1975) proposed a conceptual model, Clay Shell Model (CSM). They
 69 suggested soft clay coating on wall of grains (e.g., double layers) and the shape of pores is assumed
 70 as cylinder. The grains, clay and pores system of clayey sandstones was conceptualized in Fig. 1a.

71



72

73 **Figure 1.** (a) Clay Shell Model (CSM, modified from Al-Wardy and Zimmerman, 2004) for clayey
 74 sandstone. The clayey sandstone was conceptualized as grains, clay, and pore system; (b) Cylinder
 75 pore and the plane strain condition (vertical strain (in direction of z axis) equals to zero). The
 76 cylindrical polar coordinate was selected.

77

78 In Fig. 1a, the r is the radial distance from the center of pore to a specific point within the clay
 79 and grain domains. The r_p , r_c and r_g are the pore radius, distance from the center to the inner and
 80 outer boundaries of grains, respectively. The domain between r_p and r_c are composed of clay, and

81 the domain between r_c and r_g are composed of sand grains. The μ_g and μ_c are the shear
 82 modulus of sand grain (between r_c and r_g) and clay (between r_p and r_c), respectively. The
 83 variation of r_p versus σ_c and P_p determines the effective stress coefficient for deformability and
 84 porosity $\phi(= \frac{r_p^2}{r_g^2})$, as well as for the permeability, which will be introduced in more detail later
 85 (Section 2.1).

86 Since the elastic moduli of the clay are usually smaller than the one of grains, the influence of
 87 pore pressure on the pore radius should be larger than the influence of confining pressure. That is,
 88 this heterogeneity of clayey sandstones resulted in $\alpha > 1$ (Zoback and Byerlee, 1975). Al-Wardy
 89 and Zimmerman (2004) elaborated the CSM further following the idea proposed by Zoback and
 90 Byerlee (1975). Based on CSM (details will be introduced in Section 2.2), the effective stress
 91 coefficient α will be function of shear modulus of grains and clay, as well as the clay fraction F_c
 92 defined as follows:

$$93 \quad F_c = \frac{r_c^2 - r_p^2}{r_g^2 - r_p^2} \quad (2)$$

94 The derived α is a constant which is irrelevant to the variation of confining stress σ_c and pore
 95 pressure P_p , which is contradict to the observations of many previous studies (Todd and Simmons,
 96 1972; Coyner, 1984; Gangi and Carlson, 1996). Notably, the elastic moduli of sand grains and clay
 97 (μ_g and μ_c) are assumed as stress independent for the CSM. It is not a realistic for the elastic
 98 moduli of sand grains and clay which are stress-dependent (Mondol et al., 2008). Since the α
 99 should not be a constant but varied with changing σ_c and P_p , the equation used to calculate the
 100 effective stress would be modified slightly from Eq. (1) (e.g. Robin, 1973; Li et al., 2009; 2014), as
 101 illustrated in Eq. (3):

$$102 \quad \sigma_{eff} = \sigma_c - \alpha_{(P_p, \sigma_c)} \cdot P_p \quad (3)$$

103 The $\alpha_{(P_p, \sigma_c)}$ is a pore pressure/confining stress dependent (named as “stress dependent”
 104 thereafter) effective stress coefficient. In this paper, all of the α used thereafter represents $\alpha_{(P_p, \sigma_c)}$.

105 In this study, the stress dependency of elastic modulus of clay will be incorporated into the
 106 CSM to depict the complicate relationship between α , σ_c and P_p . We discretized the materials
 107 (sand grains and clay) into several thin rings to calculate the stress dependent elastic moduli of clay
 108 at different radial distance r to the center of pore. Using this proposed Discretized Clay Shell
 109 Model (DCSM) and the response-surface method proposed by Box and Draper (1987), the variation
 110 of α with pore pressure P_p and confining stress σ_c can be determined without much difficulties.
 111 The experimental data of stress dependent elastic moduli of kaolinite powder (Unconsolidation)
 112 documented by Mondol et al. (2008), as well as two more synthetic clay with different stress
 113 sensitive of elastic modulus, were incorporated into the DCSM to evaluate the influence of clay
 114 fraction F_c and stress dependency of elastic modulus on α .

115 Moreover, we provided a synthetic case which the variations of pore pressure P_p and confining
 116 stress σ_c at different burial depth of clayey sandstone reservoirs were given. The stress dependent
 117 effective stress coefficient α was determined using the proposed DCSM. The effective stress, as
 118 well as the permeability, can thus been calculated. The importance of relation between pore pressure
 119 P_p , confining stress σ_c , and stress dependent effective stress coefficient α to the determination of
 120 effective stress and permeability will be illustrated accordingly.

121

122 **2 Discretized Clay Shell Model (DCSM) and stress dependent effective stress coefficient α**

123 2.1 Stress independent effective stress coefficient α of permeability

124 If the effective stress coefficient α is stress independent (independent of confining stress σ_c
 125 and pore pressure P_p), Eq. (1) can be used to predict the effective stress. Under this assumption,

126 Bernabe (1987) proposed Eq. (4) to calculate the effective stress coefficient α of permeability via
 127 the permeability measurement under different pore pressure P_p and confining stress σ_c :

$$128 \quad \alpha = -\frac{\left(\frac{\partial k}{\partial P_p}\right)_{\sigma_c}}{\left(\frac{\partial k}{\partial \sigma_c}\right)_{P_p}} \quad (4)$$

129 where $\left(\frac{\partial k}{\partial P_p}\right)_{\sigma_c}$ and $\left(\frac{\partial k}{\partial \sigma_c}\right)_{P_p}$ are partial derivative of permeability k to pore pressure P_p and
 130 confining stress σ_c , respectively. Based on the Hagen-Poiseuille equation and Darcy's law, the
 131 permeability k of along a cylindrical tube can be expressed as (e.g. Civan et al., 2011; Cao et al.,
 132 2016):

$$133 \quad k = \frac{r_p^4}{8r_g^2} \quad (5)$$

134 where the r_p and r_g are the radius of pore and grains (Fig. 1a), respectively. If the r_g assumed as
 135 constant (Eulerian permeability), and insert Eq. (5) into Eq. (4), the effective stress coefficient α
 136 can be calculated using following equation:

$$137 \quad \alpha = -\frac{\left(\frac{\partial r_p}{\partial P_p}\right)_{\sigma_c}}{\left(\frac{\partial r_p}{\partial \sigma_c}\right)_{P_p}} \quad (6)$$

138 That is, the effective stress coefficient α of permeability can be determined based on the pore
 139 radius variations. The relations between the pore radius r_p , σ_c and P_p incorporate in CSM will be
 140 introduced in the following section.

141

142 2.2 Clay Shell Model (CSM) of Clayey sandstones

143 CSM conceptualized the clayey sandstones into a system with hollow cylinder pore in grains
 144 coating by clay (Fig. 1a). If the variations of r_p with σ_c and P_p can be evaluated, the α can be
 145 obtained using Eq. (6). Based on plain strain assumption (Fig. 1b) and axial symmetry, the

146 calculation is simply a 1-D problem. The only component related to r_p is the radial displacement
 147 vector $u_{(r)}$ along radius in cylindrical polar coordinate (Fig. 1b). The derivation of the relationship
 148 between $u_{(r)}$ and stress condition (σ_c and P_p) can be found in text book of elastic theory (e.g.,
 149 Sokolnikoff, 1956; Jaeger and Cook, 1979). In this paper, the basic idea was introduced briefly to
 150 better illustrate our proposed model in Section 2.3.

151 For a hollow tube model, the radial displacement $u_{(r)}$ at radial location r from the center of
 152 the tube to a specific point can be expressed as:

$$153 \quad u_{(r)} = Ar + \frac{B}{r} \quad (7)$$

154 if the material around the radial location r is homogeneous (the tube wall in Fig.1 composed of only
 155 one material). The A and B are parameters related to elastic moduli of the material composed of
 156 the tube wall. To solve A and B , the relation between radial stress σ_r and u is required as follows
 157 (Sokolnikoff, 1956):

$$158 \quad (\lambda + 2\mu) \frac{du_{(r)}}{dr} + \lambda \frac{u_{(r)}}{r} = \sigma_r \quad (8)$$

159 where λ and μ are Lamé constant and shear modulus. The radial stress σ_r at $r = r_p$ and $r = r_g$
 160 are P_p and σ_c . Therefore,

$$161 \quad (\lambda + 2\mu) \left(A - \frac{B}{r_p^2} \right) + \lambda \left(A + \frac{B}{r_p^2} \right) = P_p \quad (9)$$

$$162 \quad (\lambda + 2\mu) \left(A - \frac{B}{r_g^2} \right) + \lambda \left(A + \frac{B}{r_g^2} \right) = \sigma_c \quad (10)$$

163 The two unknowns A and B can be solved via Eqs. (9) and (10). The radial displacement
 164 when $r = r_p$ (=variation of pore radius) can be expressed by Eq. (11):

$$165 \quad u_p = Ar_p + \frac{B}{r_p} \quad (11)$$

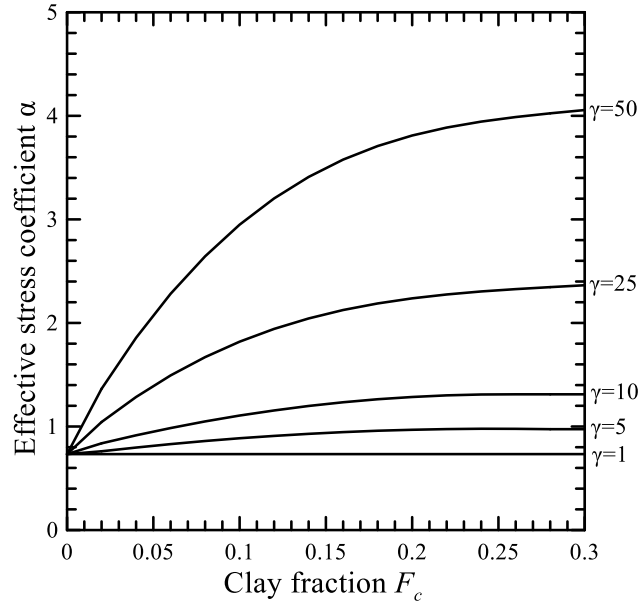
166 where u_p denotes the displacement of pore radius. The u_p can be used to calculate the variation of
 167 pore radius r_p caused by σ_c and P_p , and determine the effective stress coefficient α using Eq. (6).
 168 Notability, the α is stress independent which is a big assumption of CSM.

169 If the tube wall is composed of two materials (clay and grains, CSM in Fig. 1a), the parameters
 170 A and B for domains of clay and grains will be different. We use the A_c and B_c representing the
 171 parameters for clay domain and A_g and B_g for grain domain. Two more constrain conditions, i.e.,
 172 radial stress σ_r and displacement u are identical on the boundary of clay and grains domains when
 173 $r = r_c$, together with two boundary conditions were used to solve the four unknowns. The solved
 174 four parameters (A_c and B_c ; A_g and B_g) are function of clay fraction F_c , porosity ϕ , Poisson's
 175 ratio ν , and shear modulus ratio γ (defined in Eq. (12)), which can be found in Al-Wardy and
 176 Zimmerman (2004).

$$177 \quad \gamma = \frac{\mu_g}{\mu_c} \quad (12)$$

178 The μ_g and μ_c are shear modulus of grains and shear modulus of clay, respectively (see Fig. 1a).
 179 Fig. 2 shows the predicted α of sandstones with clay fraction F_c from 0 to 0.3 using CSM
 180 (Al-Wardy and Zimmerman, 2004). Five curves represent the different α when γ (ratio of shear
 181 modulus between grains and clay) equal to 1, 5, 10, 25, 50. The porosity ϕ of the clayey sandstones
 182 equals to 0.2. The Poisson's ratio ν of clay and grains equals to 0.25.

183



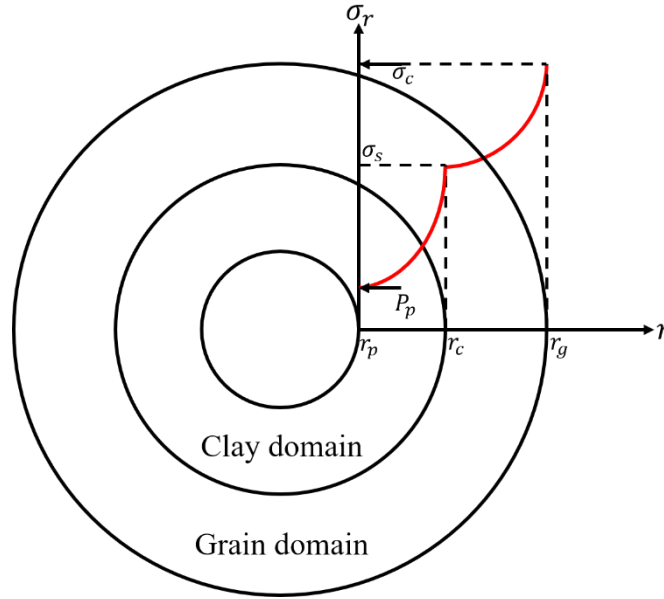
184

185 **Figure 2.** The predicted α of clayey sandstones using CSM with porosity $\phi = 0.2$, under different
 186 clay fraction F_c and shear modulus ratio γ . The Poisson's ratio $\nu = 0.25$ for grains and clay.
 187 (modified from Al-Wardy and Zimmerman, 2004)

188 When $\gamma = 1$ or $F_c = 0$, which represent a clean sandstone, the $\alpha = 0.713$. This value can be
 189 obtained analytically (Al-Wardy and Zimmerman, 2004). Generally, the effective stress coefficient
 190 α increases with increasing γ (decreases the shear modulus of clay while the shear modulus of
 191 grains is remains unchanged) and clay fraction F_c . Since the elastic moduli of clay and grains are
 192 assumed as stress-independent in CSM, the effective stress coefficient α is a constant when the F_c
 193 and γ are fixed and will not vary with changing confining stress σ_c and pore pressure P_p .

194 As aforementioned, the elastic moduli of clay are frequently stress-dependent (e.g. Mondol et
 195 al., 2008). The elastic moduli of clay at different r should not be identical since the radial stress σ_r
 196 is function of radial position r (Eq. (8) and Fig. 3).

197



198

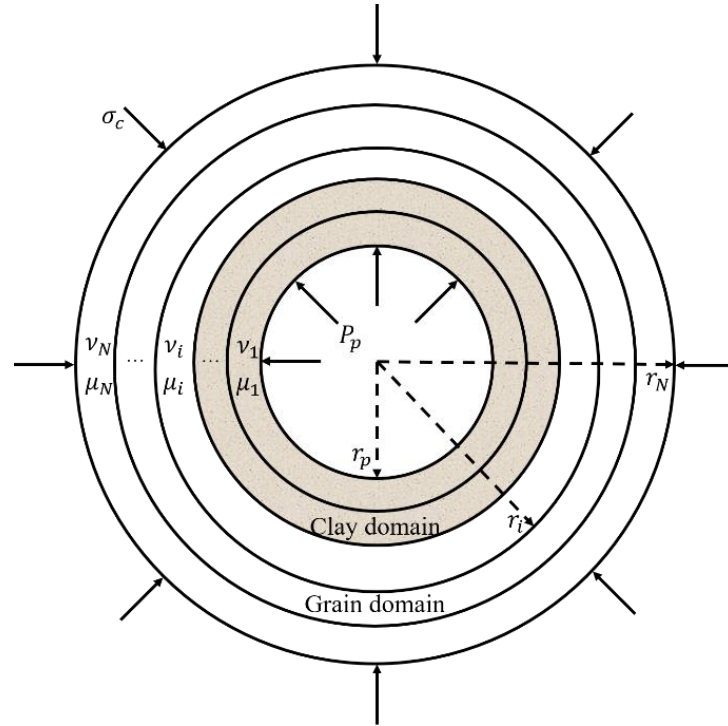
199 **Figure 3.** The radial stress distribution along the radial direction of the CSM. The gradient of radial
 200 stress for clay and grain is different for their elastic moduli are different. The two boundary stresses
 201 are P_p when $r = r_p$ and σ_c when $r = r_g$, respectively. σ_s is the radial stress when $r = r_c$. The
 202 radial stress is continuous on the boundary of clay and grains.

203

204 2.3 Discretized Clay Shell Model (DCSM)

205 According to Fig. 3, radial stress σ_r is varied with location. The elastic moduli of material at
 206 different location will be different if the elastic moduli is stress dependent. To accounts for the issue
 207 of elastic moduli heterogeneity, we discretized the clay and sand grain domains in Fig. 3 into
 208 numerous thin rings as show in Fig. 4. The r_p is the pore radius. The r_i ($i=1\sim N$) represents the
 209 outer radius of i -th ring. Here, the r_N ($i = N$) is equivalent to the outer boundary of grain domain
 210 r_g defined in previous sections. The Poisson's ratio and shear modulus of i -th ring denoted by ν_i
 211 and μ_i .

212



213

214 **Figure 4.** The Discretized Clay Shell Model (DCSM). There are N rings with different elastic moduli

215 ν_i and μ_i . The r_p is the pore radius. The r_i is the outer boundary of the i -th ring.

216

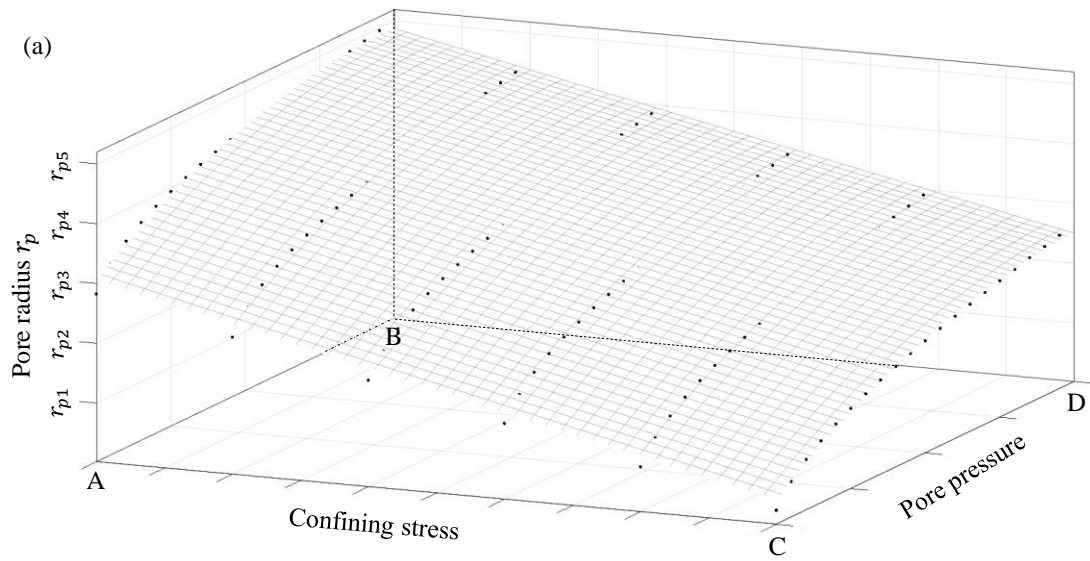
217 The parameters of A and B in Eq. (7) for each ring are different and can be denoted by A_i
 218 and B_i . Therefore, totally $2N$ unknowns need to be solved. As aforementioned, there are 4
 219 unknowns (A_c and B_c ; A_g and B_g) were solved for CSM via 2 boundary conditions (pore pressure
 220 and confining pressure applied on the inner boundary of clay domain and outer boundary of grain
 221 domain) and 2 constrain conditions (radial stress and displacement are identical on the boundary of
 222 clay and grains domains). Likewise, there are two boundary conditions and $2N-2$ constrain
 223 conditions (radial stress and displacement on boundary of i -th ring and the $(i+1)$ -th ring) in DCSM.
 224 Totally $2N$ equations were available to solve the $2N$ unknowns (A_i and B_i , $i = 1 \sim N$). The
 225 displacement of pore radius can be calculated by Eq. (11) with the determined parameters (A_1 and
 226 B_1) for the 1st ring.

227 Now the proposed DCSM can be used to calculate the displacement of pore radius u_p under
 228 different σ_c and P_p , since the radial stress dependent moduli of the clay domain will be function of
 229 both of them. However, Eq. (6) cannot be used directly for the effective stress coefficient $\alpha_{(P_p, \sigma_c)}$ is
 230 not a constant anymore. The response-surface method proposed by Box and Draper (1987) was used
 231 to determine the stress dependent effective stress coefficient for permeability under different σ_c and
 232 P_p , which will be introduced in next section.

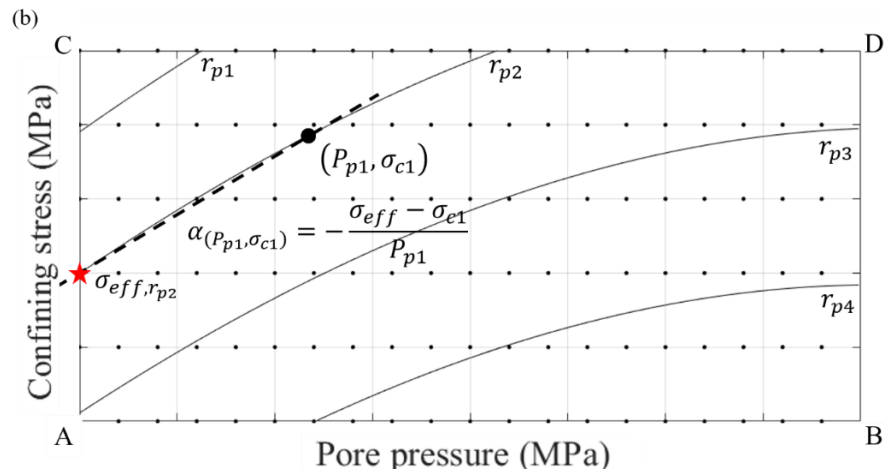
233

234 2.4 Response surface method: determining the stress dependent effective stress coefficient $\alpha_{(P_p, \sigma_c)}$

235 The response surface method proposed by Box and Draper (1987) was used in this study to
 236 determine the effective stress coefficient $\alpha_{(\sigma_c, P_p)}$. Based on Eq. (5), we can use the variations of the
 237 pore radius r_p (can be calculated by displacement of pore radius u_p determined by the proposed
 238 DCSM) due to changing of σ_c and P_p to represent the stress dependent permeability $k_{(P_p, \sigma_c)}$. The
 239 relation of pore radius r_p to the confining stress σ_c and pore pressure P_p can be depicted as a
 240 response surface and illustrated in Fig. 5a. Fig. 5b is a horizontal projection of Fig. 5a. The contours
 241 in Fig. 5b are iso- r_p curves where the pore radius under different confining stress and pore pressure
 242 are identical. Based on Eq. (5), the iso- r_p curves in Fig. 5b are iso- k curves, too. If the effective
 243 stress principle is valid, the iso- k curve can also be the iso- σ_{eff} curves.



244



245

246 **Figure 5.** Response surface method for determining the effective stress coefficient α . (a) Variations
 247 of pore radius versus changing of confining stress and pore pressure; (b) The contours of pore radius
 248 under different confining stress and pore pressure, each curve represents iso- r_p curve. The α will be
 249 the secant slope between red star and black circle.

250

251 If the effective stress coefficient α is a constant (independent of σ_c and P_p), the surface in
 252 Fig. 5a should be a plane. The iso- r_p curves in Fig. 5b will be straight lines. According to Eq. (1),
 253 the effective stress will equal to confining stress when $P_p = 0$. That is, the intercepts of the iso- r_p

254 curves and the confining stress axis are effective stress, such as the star marked on 5b. The slope of
 255 iso- r_p lines actually are effective stress coefficient α according to Eq. (1). The α would also be the
 256 same by using Eq. (6) if the surface in Fig. 5a is a plane.

257 If the effective stress coefficient α is stress dependent, the slopes of iso- r_p curves in Fig. 5b
 258 will vary with pore pressure and confining stress. According to Eq. (3), the effective stress
 259 coefficient $\alpha_{(P_{p1}, \sigma_{c1})}$ when the confining stress and the pore pressure equal to σ_{c1} and P_{p1}
 260 (circle on Fig. 5b) can be determined as follows:

$$261 \quad \alpha_{(P_{p1}, \sigma_{c1})} = -\frac{\sigma_{eff} - \sigma_{c1}}{P_{p1}} \quad (13)$$

262 since the iso- r_p curves represent the iso- σ_{eff} curves and the y-axis of stars in Fig. 5b represents the
 263 σ_{eff} . That is, the stress dependent effective stress coefficient $\alpha_{(P_p, \sigma_c)}$ is the secant slope of dash
 264 line connecting star $(0, \sigma_{eff, r_{p2}})$ and circle (P_{p1}, σ_{c1}) marked on Fig. 5b.

265

266 **3 Geometry and material properties used in DCSM**

267 3.1 Geometry and boundary conditions (confining stress and pore pressure)

268 The initial outer boundary of grain domain $r_g=25.82 \mu\text{m}$ and inner boundary of clay domain
 269 (pore radius) $r_p=10.00\mu\text{m}$ to make the porosity ϕ equals to 0.2 which is identical to the ones
 270 selected by Al-Wardy and Zimmerman (2004) for CSM. The clay and grain domains were divided
 271 into 1000 and 100 rings, respectively, for evaluating the radial stress and elastic moduli
 272 heterogeneity.

273 Several combinations of confining stress σ_c and pore pressure P_p were selected. The σ_c and
 274 P_p was both designed to increase from 2MPa to 50MPa by 2MPa of intervals.

275

276 3.2 Stress dependent elastic moduli of clay

277 Mondol et al. (2008) show that elastic moduli of clay minerals are stress dependent via the
 278 measurement of the density, P-wave and S-wave velocities of kaolinite saturated in brine and
 279 subjected to confining stress. They found the density of kaolinite increased from 2.20(g/cm³) to
 280 2.52(g/cm³), P-wave velocities increased from 1,697(m/s) to 2,470(m/s), and S-wave velocities
 281 increased from 535(m/s) to 1,014(m/s) when the confining stress increasing from 5MPa to
 282 50MPa. According to experimental results from Mondol et al. (2008), the shear modulus of kaolinite
 283 under confining stress from 5MPa to 50MPa can be determined as from 0.63GPa to 2.74GPa. The
 284 shear modulus of clay μ_c (GPa) at different location, which is essential input parameter of our
 285 DCSM, under different confining stress (radial stress σ_r (GPa) in our DCSM) can be evaluated
 286 using Eq. (14). This equation was obtained via curve fitting of the testing results of Mondol et al.
 287 (2008).

$$288 \quad \mu_c = -0.92 \times 10^2 \cdot \sigma_r^2 + 9.2 \times 10^1 \cdot \sigma_r + 4.65 \times 10^{-1} \quad 0 \leq \sigma_r \leq 0.05\text{GPa} \quad (14a)$$

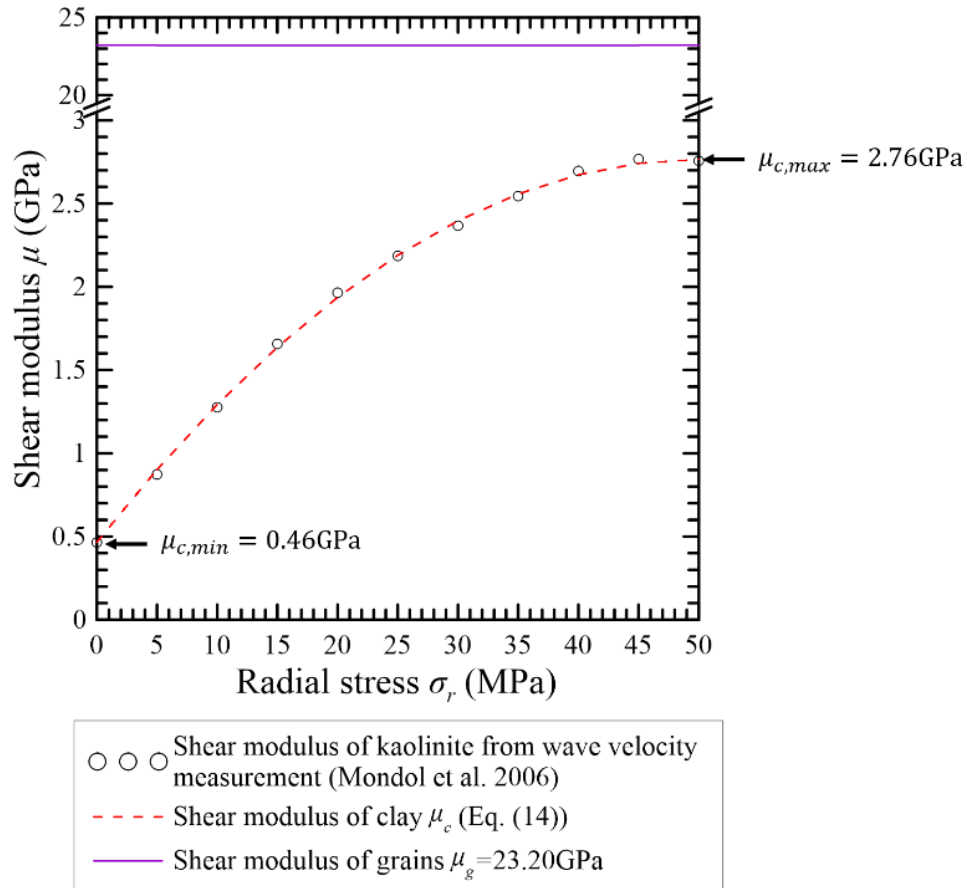
$$289 \quad \mu_c = \mu_{c,max} \quad \sigma_r > 0.05\text{GPa} \quad (14b)$$

290 In Eq. (14), $\mu_{c,max}$ is 2.76 GPa (Substitute $\sigma_r = 0.05$ GPa into Eq. (14a)) which representing
 291 the maximum value of shear modulus of clay. When $\sigma_r = 0$ GPa, a minimum shear modulus of clay
 292 ($\mu_{c,min}$) will be determined as 0.46GPa using Eq. (14a). The stress dependent shear modulus
 293 documented by Mondol et al. (2008) and the curve fitting result was shown in Fig. 6 (circles and
 294 dashed line, respectively). The determined Poisson's ratio ν of clay is ranging from 0.44 to 0.39
 295 based on the testing results of Mondol et al. (2008). In this study, the Poisson's ratio of clay was set
 296 to be 0.25, which is identical to the one used in the simulation of CSM (Al-Wardy and Zimmerman,
 297 2004) for comparison.

298

300 3.3 Elastic moduli of grains

301 In this study, we assume the elastic moduli of sand grains is stress independent. To compare our
 302 result to CSM (Fig. 2), the shear modulus of grains μ_g is 23.2GPa (illustrated in Fig. 6 together
 303 with the one of clay, μ_c) which is 50 times larger than the minimum shear modulus of clay $\mu_{c,min}$.
 304 That is, the shear modulus ratio $\gamma = 50$ when the radial stress equal to zero. The Poisson's ratio of
 305 grains ν_g equals to 0.25, which is also identical to the one of CSM.



306

307 **Figure 6.** Stress dependent shear modulus of clay. Circles denote the shear modulus of kaolinite
 308 calculated from wave measurement (Mondol et al., 2008). Dash red line denotes the stress dependent
 309 shear modulus of clay (μ_c) using curve fitting (Eq. (14)). Purple solid line denotes the shear modulus
 310 of grains (μ_g) which is stress independent (a constant, equals to 23.2GPa).

311

312 The shear modulus of each ring of clay domain was determined via a trial and error scheme.
 313 Initially, the shear modulus of each ring in clay domain equals to $\mu_{c,min}$. The DCSM program yields
 314 the radial stress distribution, and new shear modulus in clay domain can be determined. The new
 315 ones was inserted back into DCSM program to calculate the radial stress again. When the absolute of
 316 relative error ($\frac{\text{New shear modulus}-\text{Old shear modulus}}{\text{Old shear modulus}}$) less than 10^{-3} , the shear modulus of each ring of clay
 317 domain will be fixed for the calculation of r_p under different σ_c and P_p .

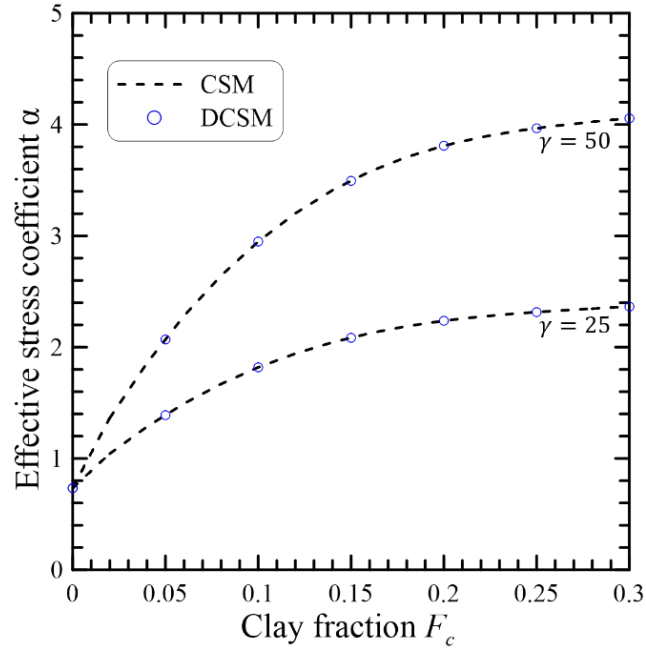
318

319 4 Results

320 4.1 Comparison of the α determined by CSM and DCSM (elastic moduli are stress independent)

321 To verify the proposed DCSM, this study compared the α documented by Al-Wardy and
 322 Zimmerman (2004) using CSM and the one calculated by the proposed DCSM. The porosity ϕ of
 323 clayey sandstone is assumed as 0.2. The Poisson's ratios of clay and grains (ν) are 0.25, the shear
 324 modulus of grains μ_g is 23.2GPa. Fig. 7 show the predicted α varied with clay fraction using CSM
 325 (dashed lines) and proposed DCSM (circles). For shear modulus ratio γ ($=\frac{\mu_g}{\mu_c}$) equals to 50, the
 326 shear modulus of clay μ_c is 0.46GPa. For shear modulus ratio γ equals to 25, the shear modulus of
 327 clay μ_c is 0.92GPa. The comparison shows the DCSM yields identical results of α predicted by
 328 CSM when the elastic moduli of clay assumed as stress-independent.

329



330

331 **Figure 7.** Comparison of the α determined by CSM (Clay Shell Model) and the proposed DCSM.

332 The dashed lines represent the effective stress coefficient α predicted by CSM when the shear

333 modulus ratio $\gamma = 25$ and 50 (shown in Fig. 2 previously). The circles are the calculated α using

334 the proposed DCSM. The parameters used are identical to ones used by Al-Wardy and Zimmerman

335 (2004). The $\mu_g = 23.2\text{GPa}$. When $\gamma = 25$, $\mu_c = 0.92\text{GPa}$. When $\gamma = 50$, $\mu_c = 0.46\text{GPa}$.

336

337 4.2 Three different stress-dependent shear modulus of clay with different stress sensitivity

338 To account for the influence of consolidation degree of clay coating on the sand grains on α of

339 clayey sandstones, this study assigned three different stress dependent shear modulus models of clay

340 with different stress sensitivity. Fig. 8a shows the three stress-dependent shear moduli of Clay 1, 2, 3.

341 The maximum shear modulus ($\mu_{c,max}$) of each clay model is 2.76 GPa. Red dashed line is Clay 1,

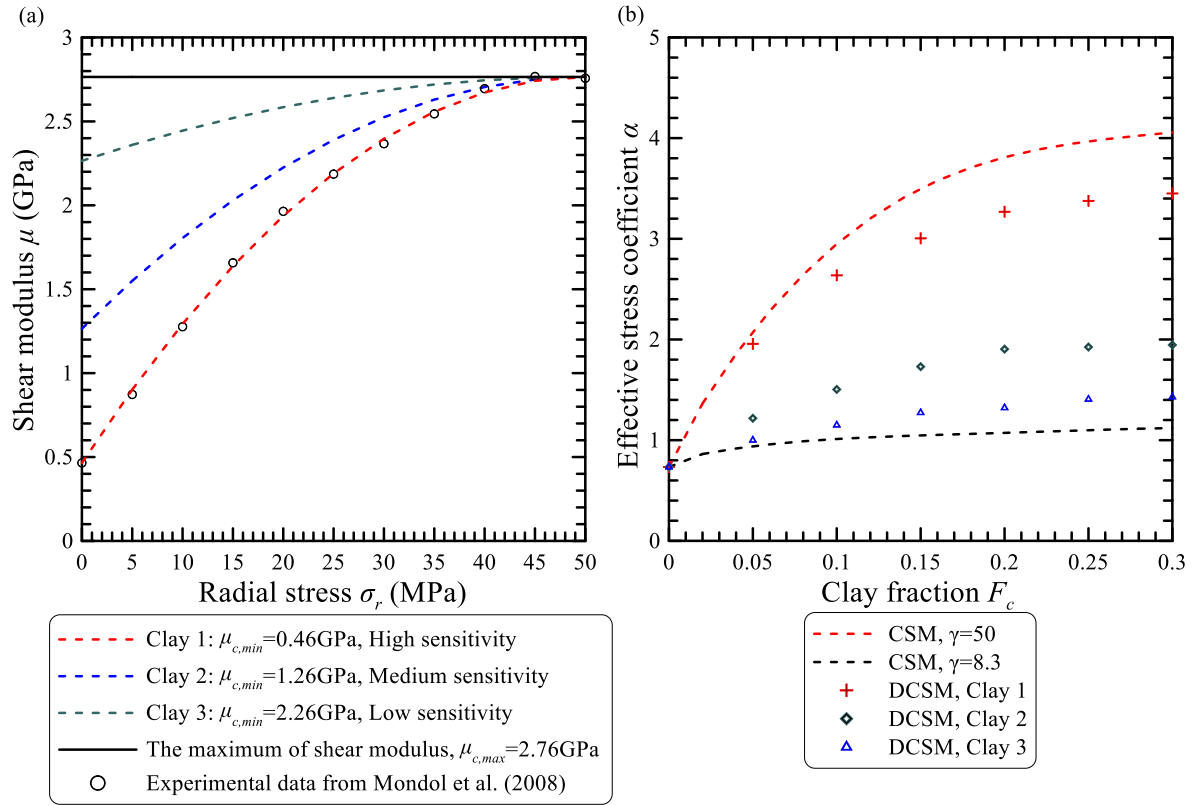
342 with $\mu_{c,min} = 0.46\text{GPa}$. Blue dashed line is Clay 2, with $\mu_{c,min} = 1.26\text{GPa}$. Green dashed line is

343 Clay 3, with $\mu_{c,min} = 2.26\text{GPa}$. The stress sensitivity of shear modulus decreased from Clay 1 to

344 Clay 3 and this could relate to the consolidation degree of clay filled in the voids of sand grains.

345 Notable, the curve of Clay 1 is identical to the curve shown in Fig. 6, which is the testing results of

346 kaolinite powder from Mondol et al. (2008).



347

348 **Figure 8.** (a) Different stress sensitivity of clay shear modulus. The maximum of shear modulus
 349 ($\mu_{c,max}$) all maintain at 2.76GPa. The $\mu_{c,min}$ of Clay 1, 2, 3 are 0.46GPa, 1.26GPa, and 2.26GPa,
 350 respectively; (b) The predicted α with $\sigma_c = 50$ MPa and $P_p = 0$ MPa using DCSM assigning
 351 shear moduli of Clay 1, 2, 3 with different stress sensitivity. The porosity (ϕ) of clayey sandstone is
 352 assumed as 0.2; The shear modulus of grains $\mu_g = 23.20$ GPa, the Poisson's ratios of clay and grains
 353 (ν) are 0.25. The predicted α for $\gamma = 50$ ($\mu_c = 0.46$ GPa, $\gamma = \frac{\mu_g}{\mu_c}$) and $\gamma = 8.3$ ($\mu_c = 2.76$ GPa,
 354 $\gamma = \frac{\mu_g}{\mu_c}$) using CSM was provided for comparison.

355

356 Fig. 8b depicts the influences of stress dependent shear modulus on α under specific stress
 357 condition with $\sigma_c = 50$ MPa and $P_p = 0$ MPa. The values of clayey sandstone porosity, the shear
 358 modulus of grains, the Poisson's ratios of clay and grains are identical to ones used in Section 4.1.
 359 The cross, diamond, and triangle symbols represent the predicted α for Clay 1, 2, and 3,
 360 respectively. Again, when $F_c = 0$, the effective stress coefficient α is 0.73 for all clay model which
 361 fits the analytical solution of CSM for clean sandstones. When F_c increases from 0 to 0.3, the α

362 increases from 0.73 to 3.45 for Clay 1 (crosses in Fig. 8b). The predicted α for $\gamma = 50$ ($\mu_c =$
 363 0.46 GPa) and $\gamma = 8.3$ ($\mu_c = 2.76$ GPa) using CSM was illustrated in dashed lines of Fig. 8b.
 364 These two lines are upper and lower bounds of α for Clay 1 since the minimum and maximum
 365 shear moduli of Clay 1 are 0.46GPa and 2.76GPa, respectively.

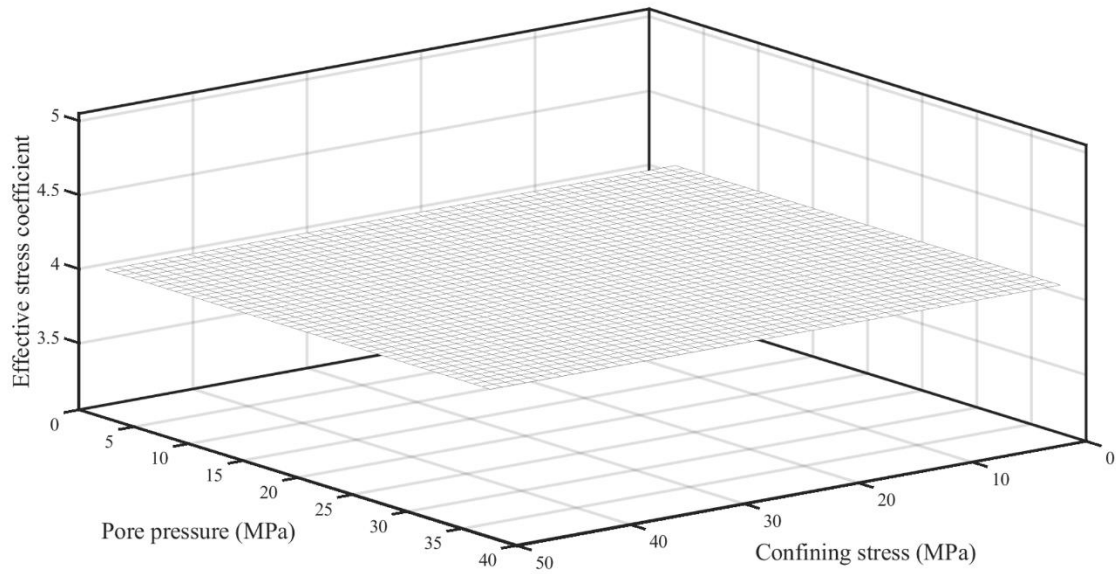
366 When the stress sensitivity of clay shear modulus decreased (Clay 2 and Clay 3), the α
 367 decreases accordingly. When F_c equals to 0.3, the α is 1.97 and 1.43 for Clay 2 (diamonds in Fig.
 368 8b) and Clay 3 (triangles in Fig. 8b), respectively. These values are smaller than the one for Clay 1
 369 ($\alpha = 3.45$ when $F_c = 0.3$). This result indicates that CSM failed to make a precise prediction if the
 370 shear modulus of clay is stress dependent with different sensitive. Moreover, the sensitivity of α to
 371 the clay fraction will be influenced by the stress dependent model of shear modulus.

372 Please note that the α predicted by DCSM can vary with σ_c and P_p , the boundary conditions
 373 used should be specified when comparing with CSM. The influence of different stress condition
 374 (combination of σ_c and P_p) will be elaborated further in Section 4.3.

375

376 4.3 Confining stress / pore pressure dependency of α

377 Figure 9 shows the predicted effective stress coefficient α by CSM is irrelevant to the
 378 confining stress σ_c and pore pressure P_p . The predicted α equals to 4.05 when the clay fraction
 379 $F_c = 0.3$ and $\gamma = 50$, which can be read from Fig. 7.

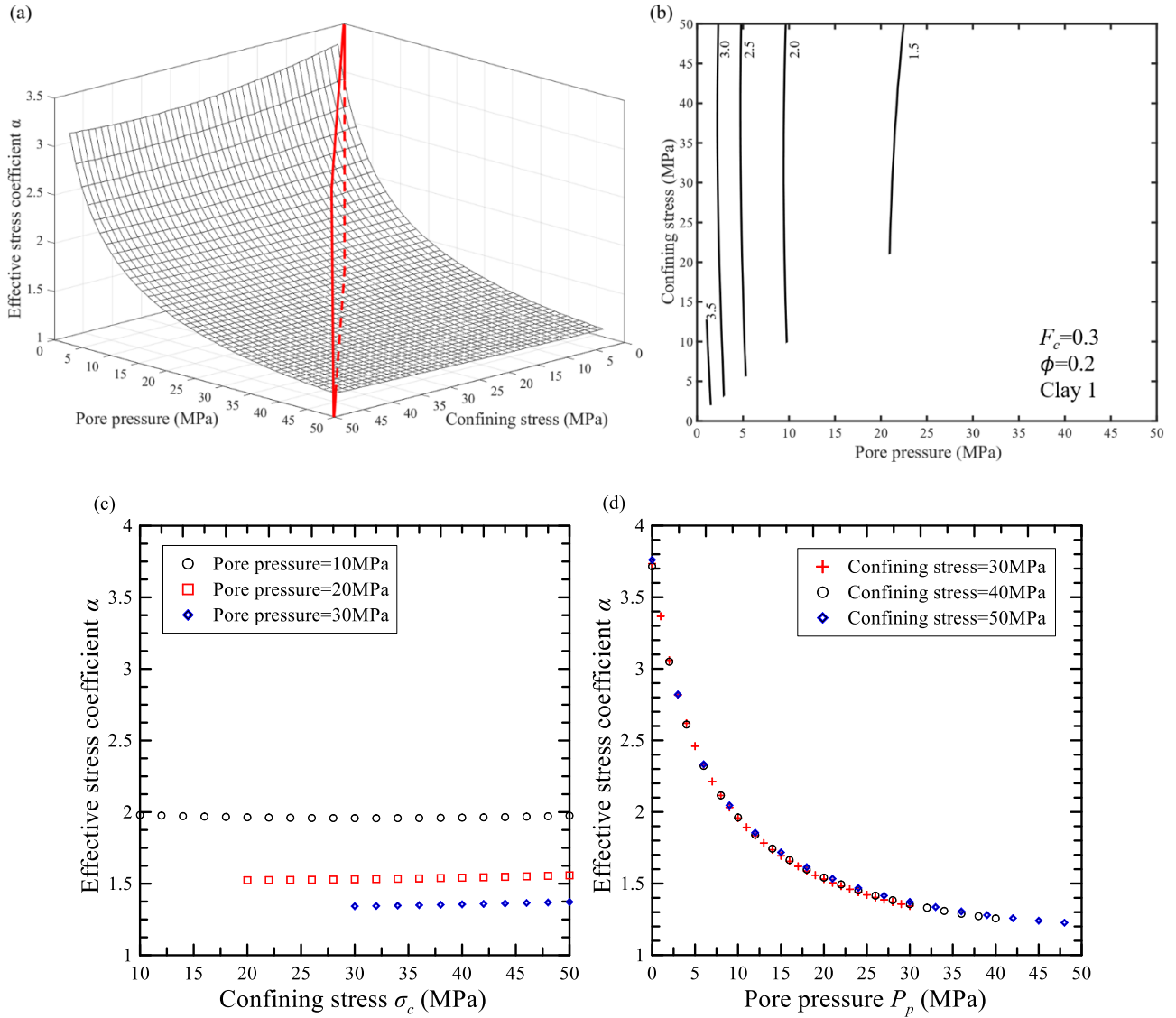


380

381 **Figure 9.** The effective stress coefficient α of clayey sandstones predicted by CSM is pore
 382 pressure/confining stress – independent. This plot shows the α equals to 4.05 with clay fraction
 383 $F_c = 0.3$ and $\gamma = 50$, which can be read from Fig. 7.

384

385 Figure 10a shows the surface depicting the stress dependent effective stress coefficient $\alpha_{(\sigma_c, P_p)}$
 386 versus σ_c and P_p (Clay 1, $\phi=0.2$, $F_c = 0.3$, Poisson's ratio of clay and grain $\nu=0.25$). The red
 387 vertical planes in Fig. 10a represents the conditions where the pore pressure P_p equals to the
 388 confining stress σ_c . This study only focuses on the conditions where P_p lower than σ_c . To visualize
 389 the influence of P_p and σ_c on α two dimensionally, Fig. 10b shows the contours of Fig. 10a.
 390 Figure 10c shows the relation between $\alpha_{(\sigma_c, P_p)}$ and σ_c when P_p remains unchanged (10, 20, 30
 391 MPa). Figure 10d shows the $\alpha_{(\sigma_c, P_p)}$ under different P_p when $\sigma_c=30, 40, 50$ MPa.



392

393

394 **Figure 10.** (a) The effective stress coefficient α of clayey sandstones (Clay 1, $\phi=0.2$, $F_c = 0.3$,
 395 Poisson's ratio of clay and grains $\nu = 0.25$) predicted by the proposed DCSM is pore
 396 pressure/confining stress – dependent. The red vertical planes representing the conditions where the
 397 pore pressure P_p equals to the confining stress σ_c ; (b) The contours of stress coefficient α derived
 398 from the surface shown in Fig. 10a; (c) The α changes with the confining stress. Black circles, red
 399 squares and blue diamonds denote the α changes with the pore pressure when the confining stress is
 400 10MPa, 20MPa, and 30MPa, respectively; (d) The α changes with the pore pressure. Red cross and
 401 black circles, and blue diamonds denote the α changes with the pore pressure when the confining
 402 stress is 30MPa, 40MPa and 50MPa, respectively.

403

404 Fig. 10b shows the contours are almost parallel to the y-axis when pore pressure is lower than
 405 15MPa. It indicates the influence of confining stress to the effective stress coefficient α is relatively
 406 minor. This can be read from Fig. 10c, too. Figure 10d shows the α is significantly influenced by
 407 pore pressure. When the pore pressure is lower than 1MPa, the α can be as high as 3.70 but the α
 408 decreases rapidly with increasing pore pressure (Fig. 10d). When pore pressure is larger than 25MPa,
 409 the α will be less than 1.5.

410

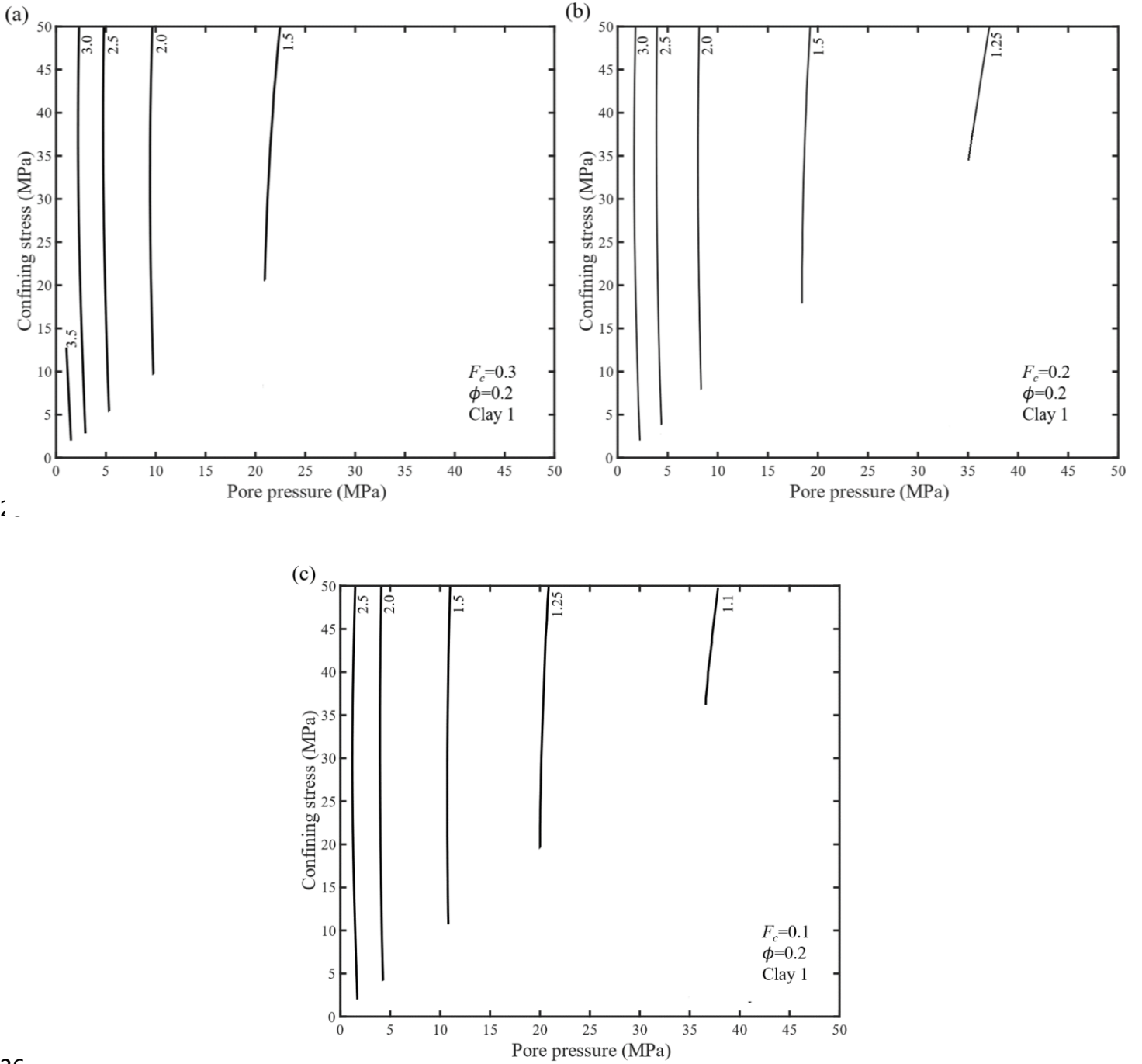
411 4.4 Influence of dominating factors on effective stress coefficient α of clayey sandstones under 412 different combination of confining stress and pore pressure

413 This section try to illustrate the influence of different factors considered in the proposed DCSM
 414 on effective stress coefficient α . Three factors are analyzed: (1) clay fraction F_c ; (2) stress
 415 dependent shear modulus the clay (Clay 1, Clay 2, and Clay 3 in Fig. 8a); and (3) porosity ϕ , under
 416 different combination of confining stress σ_c and pore pressure P_p .

417

418 4.4.1 Influence of clay fraction on α under different stress condition

419 Fig. 11a, 11b, and 11c shows the influence of clay fraction (F_c) on α , which the coating
 420 material on grain is Clay 1 with $\phi=0.2$. It is obviously to find that the α subjected to P_p decreased
 421 with decreasing F_c . When $F_c = 0.3$, the range of the α changed from 3.70 to 1.22. However, the
 422 range of α changed only from 2.71 to 1.06 when $F_c = 0.1$. Fig. 11a, 11b, 11c finds the influence of
 423 confining stress to α is still insignificant when pore pressure is smaller than 20MPa. In all cases, the
 424 α are always larger than 1.



426

427

Figure 11. Effective stress coefficient α versus confining stress σ_c and pore pressure P_p of the clayey sandstones for different clay fraction (F_c). The porosity $\phi=0.2$, Poisson's ratio of clay and grains $\nu = 0.25$, the shear modulus of grains $\mu_g=23.2\text{GPa}$. (a) $F_c = 0.3$, Clay 1 (refer to Fig. 8a which $\mu_{c,max} = 2.76\text{GPa}$, and $\mu_{c,min} = 0.46\text{GPa}$); (b) $F_c = 0.2$, Clay 1; (c) $F_c = 0.1$, Clay 1.

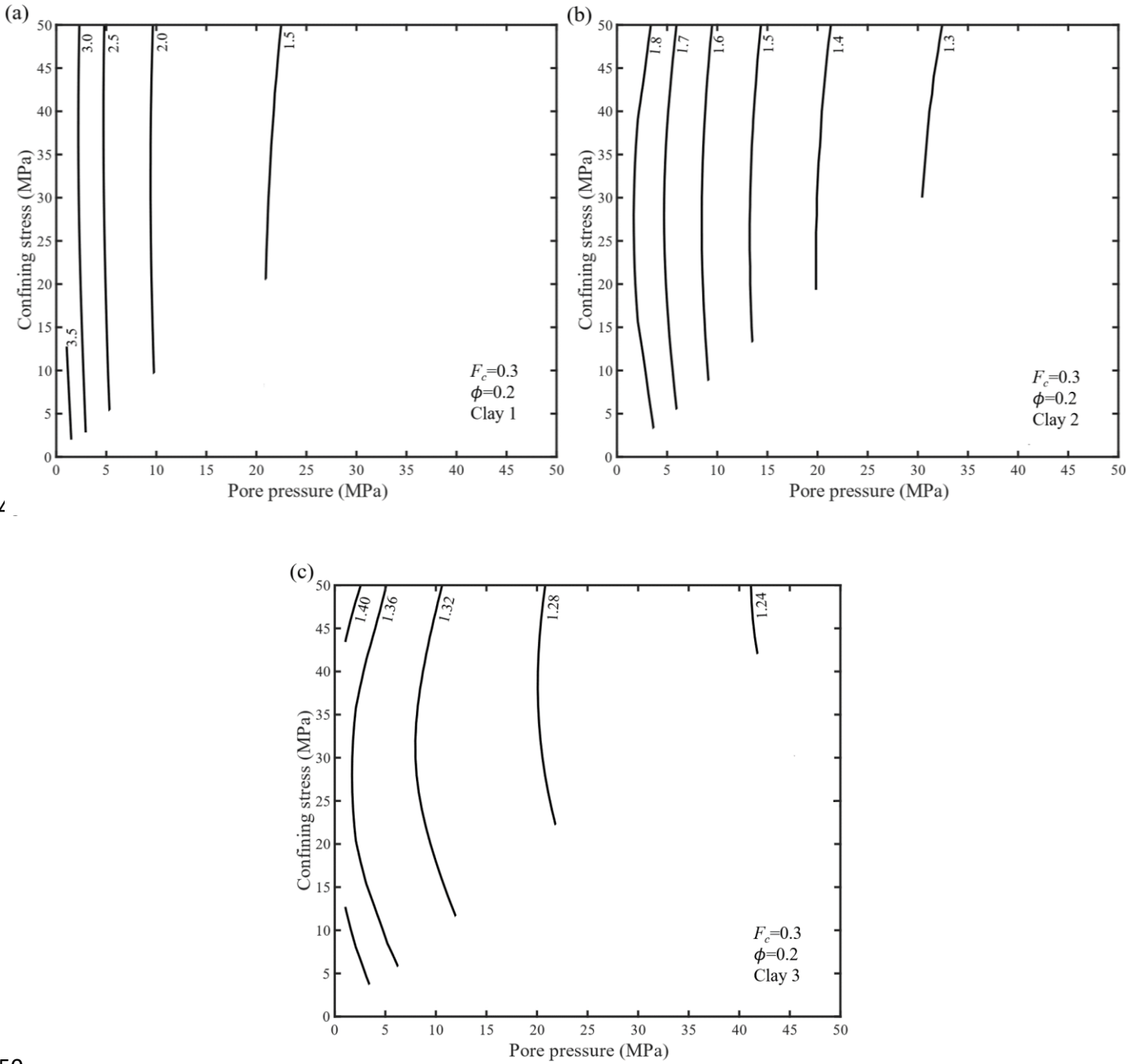
431

432 4.4.2 Influence of stress dependent shear modulus of clay on α under different stress condition

433 The stress dependency of clay materials on the effective stress coefficient α has already been
434 illustrated in Fig. 8. This section try to depict the combined effect of pore pressure, confining stress,
435 and the stress dependency of clay materials (see Fig. 8a), on the effective stress coefficient α . The
436 clay fraction F_c is assumed as 0.3 and the porosity ϕ is 0.2.

437 The evaluated results are illustrated in Figs. 12a, 12b, 12c. Fig. 12a is the effective stress
438 coefficient for Clay 1 (high stress sensitivity, low consolidation degree). The value of the α changes
439 from 3.70 to 1.22. Fig. 12b is the result for Clay 2 (middle stress sensitivity, middle consolidation
440 degree). It shows the α are smaller than ones of Clay 1. The value of the α changes from 1.97 to
441 1.21. The material in Fig. 12c is Clay 3 (low stress sensitivity, high consolidation degree). It shows
442 the α is the smallest in all of clay models. The value of the α changes from 1.45 to 1.20. It is
443 obviously to find that the α decreased with increasing consolidation degree of clay. Moreover, the
444 influence of confining stress to α will be affected by the consolidation degree (stress sensitivity) of
445 clay. In Fig. 12a, the contours lines of α approach to vertical straight lines. It implies that the α is
446 not strongly influenced by confining stress. However, the curves in Fig. 12c deviating from the
447 vertical lines and the influence of confining stress becomes significant.

448



44

450

451 **Figure 12.** Effective stress coefficient α versus confining stress σ_c and pore pressure P_p of the
 452 clayey sandstones for different Clay model (refers to Fig. 8a). The fraction of clay $F_c = 0.3$, the
 453 porosity $\phi = 0.2$, the Poisson's ratio of clay and grains $\nu = 0.25$, and the shear modulus of grains
 454 $\mu_g = 23.2 \text{ GPa}$. (a) Clay 1: The $\mu_{c,max} = 2.76 \text{ GPa}$ and $\mu_{c,min} = 0.46 \text{ GPa}$; (b) Clay 2: The
 455 $\mu_{c,max} = 2.76 \text{ GPa}$ and $\mu_{c,min} = 1.26 \text{ GPa}$.; (c) Clay 3: The $\mu_{c,max} = 2.76 \text{ GPa}$ and $\mu_{c,min} =$
 456 2.26 GPa .

457

458 4.4.3 Influence of porosity on α under different stress condition

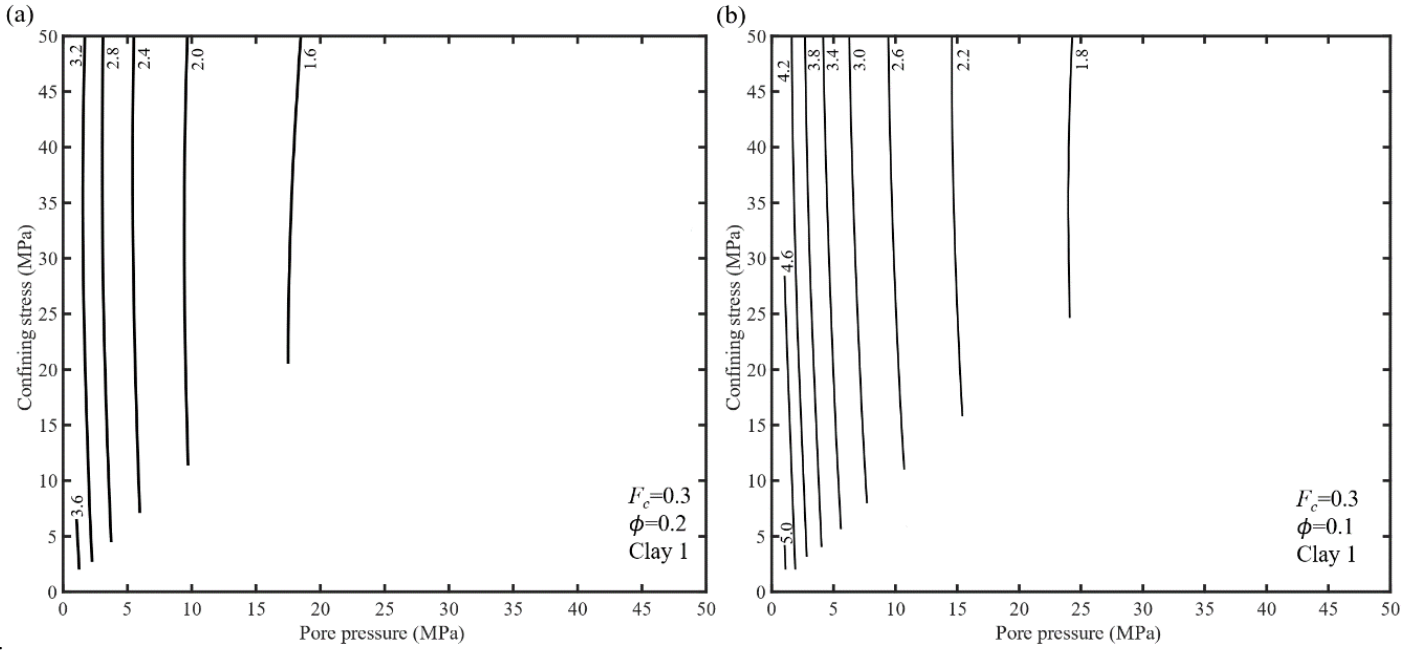
459 Figure 13a and 13b depict the difference of predicted α of clayey sandstones when the porosity
460 ϕ equals to 0.20 and 0.10, respectively. The clay model is Clay 1 with $F_c=0.3$. We find that the α
461 increases with decreasing porosity. For $\phi=0.20$, the contour values of α ranges from 3.6 to 1.6. For
462 $\phi=0.10$, the contour values of α ranges from 5.0 to 1.8. The spacing of contours of α under
463 constant confining stress (parallel to the axis of pore pressure) when $\phi=0.10$ is smaller than the ones
464 when $\phi=0.20$, indicating a high value of α for porous clayey sandstones and the dropping of α
465 with increasing pore pressure will be significant. Please note that when the clay fraction was fixed,
466 the porosity is related to the pore size directly. The pore radius (r_p) decreases with decreasing
467 porosity ϕ when the outer boundary of grains and clay fraction F_c are fixed. Smaller the pore
468 radius is, the thicker the clay domain is. It results in increasing effective stress coefficient α . It
469 should be note here that the pore volume within the clay is neglected in this study for calculating
470 porosity. That is, the true porosity for all of the synthetic clayey sandstones should be higher.

471

472

473

474



475

476 **Figure 13.** Effective stress coefficient α versus confining stress σ_c and pore pressure P_p of the
 477 clayey sandstones for different porosity (ϕ). The Poisson's ratio of clay and grains $\nu = 0.25$. The
 478 shear modulus of grains $\mu_g = 23.2 \text{ GPa}$. The clay fraction $F_c = 0.3$ and the coating clay is Clay 1. (a)
 479 $\phi = 0.2$; and (b) $\phi = 0.10$.

480

481 5 Discussions

482 5.1 The controversial measurement results of α for clayey sandstones

483 5.1.1 Should the α increase or decrease with increasing confining stress?

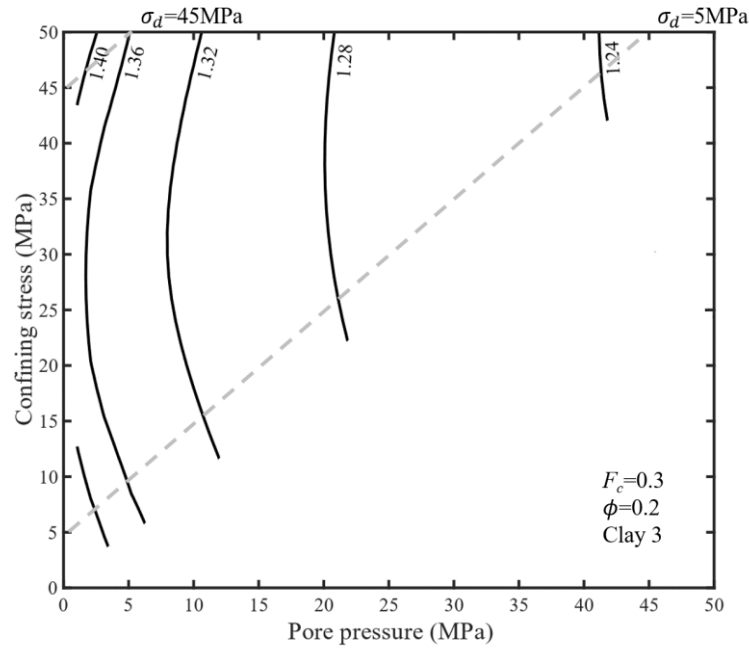
484 Quite a lot of experimental results shows the α of clayey sandstones decrease with increasing
 485 confining stress (e.g. Siggins and Dewhurst, 2003; Abass, et al., 2009; Dassanayake et al., 2015;
 486 Ingraham et al., 2017) when the pore pressure is fixed at relative low pressure (such as 5MPa). On
 487 the contrary, Ghabezloo et al. (2009) found the α of limestone (clay coating on the pore wall)
 488 increase with increasing confining stress. This controversial results can be explained by the different
 489 combination of pore pressure and confining stress. In Fig. 12c, the α will increase with increasing

490 confining stress when the confining stress below certain threshold (~25 MPa when the pore pressure
491 fixed at 5MPa). While the α start to decrease with increasing confining stress when the confining
492 stress goes above this threshold. It is indicated that the coupling effects of pore pressure and
493 confining stress on effective stress coefficient α . The traditional CSM fail to depict this phenomenon.
494

495 5.1.2 Can differential pressure be used to predict α ?

496 Some previous studies (e.g., Siggins and Dewhurst, 2003; Abass, et al., 2009) used differential
497 pressure σ_d (confining stress minus pore pressure) to evaluate the effective stress coefficient α .
498 This could oversimplify the combining effect of confining stress and pore pressure on α . Using the
499 calculated contours of α in Fig. 12c as an example, the iso-differential pressure (σ_d) lines (two gray
500 dashed lines) intersected with different contour lines of α , indicating that the differential pressure
501 σ_d could not be a single quantity to evaluate the effective stress coefficient α . However, it is
502 interesting to observed that when the σ_d increased from 5MPa to 45MPa, the variation of α along
503 the iso- differential pressure (σ_d) lines reduced significantly. It indicates that when the differential
504 pressure increased, the simplification to use σ_d for evaluating α could induce minor errors.

505



506

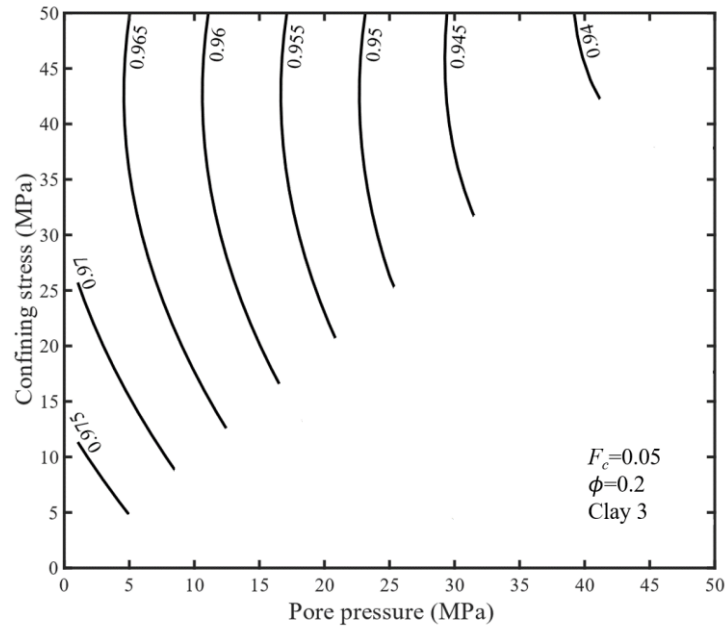
507 **Figure 14.** The contours of effective stress coefficient α shown in fig. 12c. The dashed line
 508 represent the iso-differential stress σ_d , which are 5MPa and 45MPa, respectively.

509

510 5.1.3 Why the $\alpha < 1$ for some high clay content sandstones?

511 Al-Wardy and Zimmerman (2004) found the α could be up to 5.5 for Stainton sandstone.
 512 However, the α measured in some previous studies (e.g. Ingraham et al., 2017) were smaller than 1
 513 even the clay fraction approach to 20%. The quantitative evaluation of clay content could be an
 514 arguable point. Al-Wardy and Zimmerman (2004) use SEM to identify the clay fraction but the Laser
 515 Particle Size Analyzer (LPSA) was used by Ingraham et al. (2017). The SEM image can
 516 appropriately evaluate the content of clay coating on the pore wall. However, the clay content
 517 characterized by the LPSA cannot guarantee the presence of clay is coated on the pore wall. We
 518 suspect the high clay content identified by LPSA could include the grains contain clay mineral,
 519 together with the clay filled within the pores (which should be used to evaluate the clay fraction F_c
 520 of CSM and DCSM). That is, the clay fraction (parameters of CSM and DCSM) of the clayey
 521 sandstones which documented by the papers showing $\alpha < 1$ could be lower than expected. It has

522 already been indicated that the predicted effective stress coefficient α via CSM could be lower than
 523 1 when the clay fraction is low enough (Fig. 2). Our DCSM predicted α of clayey sandstones below
 524 1 as well (Fig. 15) if the clay fraction is low enough ($F_c=0.05$) and high consolidation degree (Clay 3,
 525 high value and low stress sensitivity of clay shear modulus) clay filled within the pores.
 526



527

528 **Figure 15.** The effective stress coefficient α is always below 1 when $F_c = 0.05$ (low clay fraction)
 529 and Clay 3 (high consolidation degree with low stress sensitivity of clay shear modulus which
 530 $\mu_{c,max} = 2.76\text{GPa}$ and $\mu_{c,min} = 2.26\text{GPa}$; Fig. 8a) was selected. The porosity of clayey sandstone
 531 $\phi=0.2$; Poisson's ratio of clay and grains $\nu = 0.25$; the shear modulus of grains $\mu_g=23.2\text{GPa}$.

532

533 The micro cracks within the samples could be another influential factors on the high variability
 534 of the measured α . Li et al (2009) measured the effective stress coefficient α for permeability of 23
 535 clayey sandstones under different combinations of stress conditions. The results shows α ranged
 536 from 1.33 to 0.86. However, some of the α under different σ_c and P_p could as low as 0.3. Li et al
 537 (2009) explained the fractures and micro-fractures accounts for the low α . There are many fractures
 538 in samples used in Abass et al. (2009), Dassanayake et al. (2015), and Ingraham et al. (2017) who

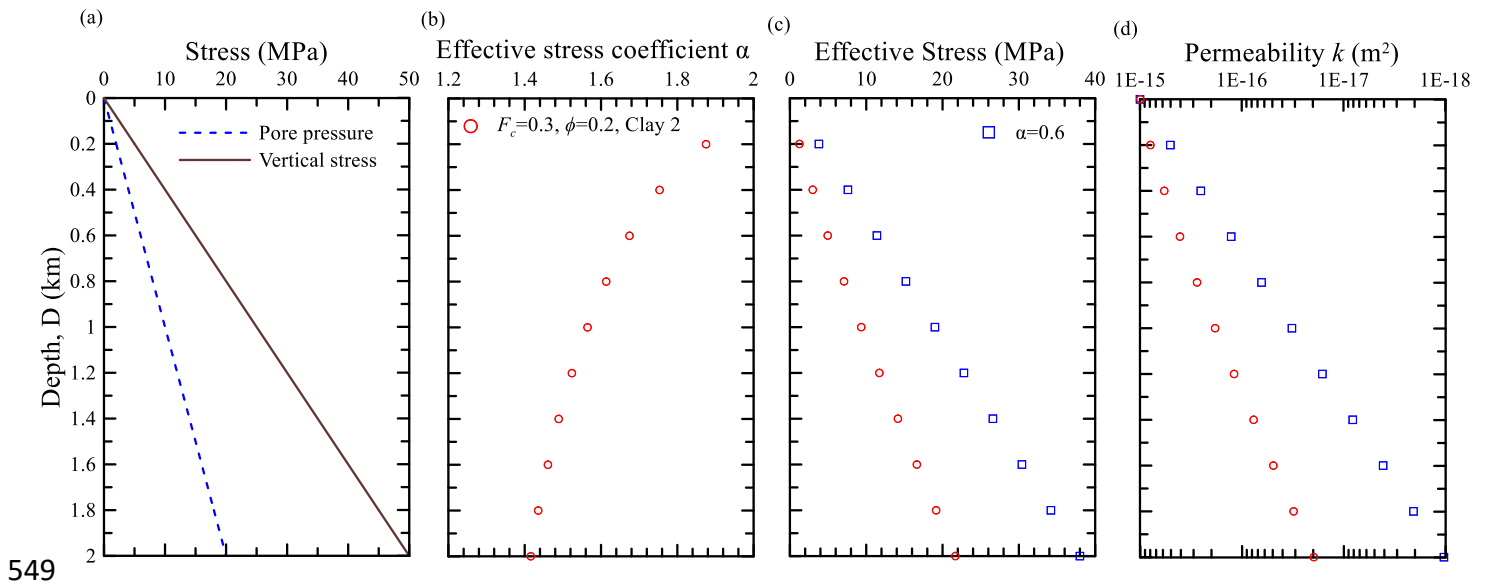
539 also found α of clayey sandstones for permeability are smaller than 1.

540

541 5.2 A synthetic case to illustrate how the permeability-depth relation can be predicted via DCSM

542 We used a synthetic clayey sandstone reservoirs to illustrate the influence of σ_c and P_p on the
 543 effective stress coefficient and the predicted permeability-depth relation using effective stress. The
 544 unit weight of sandstones $\gamma_w = 25$ (kN/m^3). The total vertical burial stress at depth D , which was
 545 used to represent the confining stress $\sigma_c (= \gamma_w \times D)$ in this study, can be determined. The pore
 546 pressure increase with burial depth and following the hydrostatic line. The total vertical stress
 547 (confining stress) and pore pressure distribution can be found in Fig. 16a.

548



549 **Figure 16.** (a) Imaged case that excess pore pressure increased with burial depth. (Assume the
 550 average of unit weight of formation is 25 kN/m^3); (b) The effective stress coefficient α changed
 551 with burial depth determined by DCSM ($F_c = 0.3, \phi = 0.2, \text{Clay 2}$); (c) The prediction of effective
 552 stress by DCSM, and condition of $\alpha = 0.6$; (d) The prediction of permeability based on exponential
 553 law proposed by David et al. (1994) (Eq. 15). The stress sensitivity coefficient $q=0.018$, and
 554 permeability at atmosphere pressure $k_o=1$ Darcy ($10^{-15}m^2$).

556

557 Based on our proposed DCSM, the α can be determined by pore pressure and the confining
 558 stress (vertical stress). The stress dependent model Clay 2 (Fig. 8a) was selected. The porosity (ϕ) of
 559 the clayey sandstones is 0.2 and the clay fraction $F_c=0.3$. Fig. 16b shows the variation of effective
 560 stress coefficient α determined by DCSM (dropped from 1.88 to 1.42 from 0.2 km to 2.0 km). The
 561 red symbols in Fig. 16c represents the effective stress which calculated by Eq. (3) and the determined
 562 α . The blue square symbols are the effective stress assumed $\alpha = 0.6$ (Abass et al., 2009).

563 This study uses Eq. (15) proposed by David et al. (1994) to model the stress dependent
 564 permeability.

$$565 \quad k = k_o e^{-q(\sigma_{eff} - \sigma_o)} \quad (15)$$

566 where k_o is permeability at atmosphere pressure, σ_o , which equals to 0.1 MPa, and q is the stress
 567 sensitivity coefficient of permeability. We selected $q=0.018$ which is identical to the parameter for
 568 Rothbach sandstone (clay fraction $F_c=12\%$, $\phi=19.9\%$) in David et al. (1994). The k_o was assumed
 569 as 1 Darcy ($=10^{-15}m^2$).

570 In Fig. 16d, the variations of permeability k at different burial depth are calculated via Eq. (15)
 571 using different effective stresses showing in Fig. 16c. Generally, the α determined by DCSM is
 572 larger than 1. This makes the predicted effective stress smaller than the one calculated under the
 573 condition of $\alpha=0.6$. It indicates that the k will be underestimated if the assumption of $\alpha=0.6$ is
 574 adopted. The maximum discrepancy (at burial depth 2.0km) is about one order of magnitude. It is
 575 interesting to note that when the overpressure condition exits, the effective stress α determined by
 576 DCSM would be more approached to 1 and the underestimated permeability will be insignificant if
 577 we assume $\alpha = 1$.

578

579 **6 Conclusions**

580 This study modifies Clay Shell Model (CSM) by incorporating the confining stress / pore
 581 pressure dependent elastic modulus of clay into discretizing multi-layers clay domain. The proposed

582 Discretized Clay Shell Model (DCSM) determines α under different stress conditions using
583 response surface method. The parametric study and the prediction of permeability-depth relation
584 using synthetic case illustrate the superior features of the proposed DCSM to the traditional CSM.

585 The main findings are summarized as follows:

- 586 1. The predicted effective stress coefficient α form a concaving upward surface in the pore
587 pressure-confining stress space using DCSM while the traditional CSM yields a constant when the
588 material properties of clay and grain remain unchanged.
- 589 2. The curvature of the concave surface along the pore pressure axis is smaller (flatter) than the one
590 along the confining stress axis, indicating that the influence of pore pressure on α is stronger than
591 the one of confining stress. When the confining stress keeping as a constant, the predicted α
592 decreased with increasing pore pressure. The decreasing trend is stronger under low pore pressure
593 than the one under high pore pressure. This feature can be observed from the horizontal distance
594 between contour lines increased with increasing pore pressure. It is interesting to note that the
595 predicted α could decrease first with elevated confining stress and start to increase when the
596 confining stress goes up to a threshold value, if the pore pressure remains unchanged. This trend
597 can be observed from the curved contour lines of α .
- 598 3. The stress dependent shear modulus of clay coating on the grain dominating the variability of the
599 predicted α . When the clay was normally consolidated (Clay 1 model) and the compressibility is
600 large, the value and variability will be large and significant. On the contrary, the predicted α of
601 low stress sensitivity with low compressibility (Clay 3 model) will approach to 1 and the
602 variability is lowest among the three clay model. This result indicates that the effective stress
603 principal proposed by Terzaghi (1943) (i.e., $\alpha = 1$) can be invalidate for young, clayey sandstones.
- 604 4. Same with the prediction results via CSM, the effective stress coefficient α predicted by the
605 proposed DCSM will increase with increasing clay fraction. The predicted α could be lower than
606 1 for low clay content sandstones under different combination of pore pressure and confining
607 stress. The variability of predicted α under different combination of pore pressure and confining

- 608 stress using DCSM will increase when the clay fraction increased. That is, the influence of stress
609 dependency of clay shear modulus should not be neglected when the clay fraction is high.
- 610 5. The effective stress coefficient of clayey sandstones increases with decreasing porosity. The
611 decreased rate of α under low pore pressure will be larger when the porosity of clayey sandstones
612 is lower. This is actually related to the pore size and the thickness of clay domain.
- 613 6. The applicability for using differential stress σ_d (Difference of confining stress and pore pressure)
614 to predict the effective stress coefficient α depends on the combination of confining stress and
615 pore pressure. It seems that this approach can only be valid under high confining stress, low pore
616 pressure.
- 617 7. The determination of clay fraction of clayey sandstones should be conducted with caution. From
618 the aspect of DCSM prediction, the SEM approach could superior than the XRD approach for the
619 former one can only include the clay coating on the pore wall. The presence of micro-cracks
620 accounts for the low measured α .
- 621 8. The synthetic case shows the predicted permeability using the proposed DCSM is significantly
622 larger than the predicted one assuming $\alpha=0.6$. The maximum discrepancy of predicted
623 permeability at burial depth 2.0 km could be one order of magnitude. However, when overpressure
624 exist, the predicted α will approach to one and the effective stress principle ($\alpha=1$) assumption
625 will not induce significant error.

626

627 **Acknowledgments**

628 This research was supported by Taiwan Ministry of Science and Technology
629 (MOST108-2638-E-008-001-MY2 and MOST107-2116-M-008-001-MY3). This work was also
630 financially supported by Earthquake-Disaster & Risk Evaluation and Management
631 Center (E-DREaM) from The Featured Areas Research Center Program within the framework of the
632 Higher Education Sprout Project by the Ministry of Education (MOE) in Taiwan. The data published

633 in the literatures used in this study are available through Al-Wardy and Zimmerman (2004), Mondol
634 et al. (2008) and David et al. (1994). All the parameters used in the equations and modeling program
635 are explained in the text. All the data of stress dependent effective stress coefficient with different
636 clay fraction, porosity, and consolidation degree of clay are provided as supporting information.

637

638 **Reference**

639 Abass, H. H., Al-Tahini, A. M., Abousleiman, Y., & Khan, M. R. (2009). *New technique to*
640 *determine Biot coefficient for stress-sensitive dual-porosity reservoirs*. Paper presented at
641 SPE Annual Technical Conference and Exhibition, Society of Petroleum Engineers.
642 <https://doi.org/10.2118/124484-MS>

643 Al-Wardy, W., & Zimmerman, R. W. (2004). Effective stress law for the permeability of clay-rich
644 sandstones. *Journal of Geophysical Research*, *109*(B4).
645 <https://doi.org/10.1029/2003JB002836>

646 Bernabe, Y. (1987). The effective pressure law for permeability during pore pressure and confining
647 pressure cycling of several crystalline rocks. *Journal of Geophysical Research*, *92*(B1),
648 649-657. <https://doi.org/10.1029/JB092iB01p00649>

649 Berryman, J. G. (1992). Exact effective-stress rules in rock mechanics. *Physical Review A*, *46*(6),
650 3307–3311. <https://doi.org/10.1103/PhysRevA.46.3307>

651 Box, G. P., & Draper, N. P. (1987). *Empirical Model-Building and Response Surfaces*, John Wiley,
652 New York.

653 Breckels, I. M., & van Eekelen, H. A. M. (1982). Relationship between horizontal stress and depth in
654 sedimentary basins. *Journal of Petroleum Technology*, *34*, 2191-2198.
655 <https://doi.org/10.2118/10336-PA>

- 656 Cao, P., Liu, J., & Leong, Y. K. (2016). General gas permeability model for porous media: bridging
657 the gaps between conventional and unconventional natural gas reservoirs. *Energy & Fuels*,
658 30(7), 5492-5505. <https://doi.org/10.1021/acs.energyfuels.6b00683>
- 659 Civan, F., Rai, C. S., & Sondergeld, C. H. (2011). Shale-gas permeability and diffusivity inferred by
660 improved formulation of relevant retention and transport mechanisms. *Transport in porous*
661 *media*, 86(3), 925-944. <https://doi.org/10.1007/s11242-010-9665-x>
- 662 Coyner, K. B. (1984). Effects of stress, pore pressure and pore fluid on bulk strain, velocity, and
663 permeability in rocks, (Doctoral dissertation). Massachusetts Institute of Technology,
664 Cambridge, U.K.
- 665 Cui, X., Bustin, R. M., & Chikatamarla, L. (2007). Adsorption-induced coal swelling and stress:
666 implications for methane production and acid gas sequestration into coal seams. *Journal of*
667 *Geophysical Research: Solid Earth*, 112(B10). <https://doi.org/10.1029/2004JB003482>
- 668 Dassanayake, A. B. N., Fujii, Y., Fukuda, D., & Kodama, J. I. (2015). A new approach to evaluate
669 effective stress coefficient for strength in Kimachi sandstone. *Journal of Petroleum Science*
670 *and Engineering*, 131, 70-79. <https://doi.org/10.1016/j.petrol.2015.04.015>
- 671 David, C., Wong, T. F., Zhu, W., & Zhang, J. (1994). Laboratory measurement of
672 compaction-induced permeability change in porous rocks: implication for the generation and
673 maintenance of pore pressure excess in the crust. *Pure and Applied Geophysics*, 143(1),
674 425-456. <https://doi.org/10.1007/BF00874337>
- 675 Dong, J. J., Hsu, J. Y., Wu, W. J., Shimamoto, T., Hung, J. H., Yeh, E. C., Wu, Y. H., & Sone, H.
676 (2010). Stress-dependence of the permeability and porosity of sandstone and shale from
677 TCDP Hole-A. *International Journal of Rock Mechanics and Mining Sciences*, 47(7),
678 1141-1157. <https://doi.org/10.1016/j.ijrmms.2010.06.019>

- 679 Engelder, T., & Fischer, M. P. (1994). Influence of poroelastic behavior on the magnitude of
680 minimum horizontal stress, S_h in overpressured parts of sedimentary basins. *Geology*, 22(10),
681 949-952. [https://doi.org/10.1130/0091-7613\(1994\)022<0949:IOPBOT>2.3.CO;2](https://doi.org/10.1130/0091-7613(1994)022<0949:IOPBOT>2.3.CO;2)
- 682 Gaarenstroom, L., Tromp, R. A. J., de Jong, M. C., & Brandenburg, A. M. (1993). *Overpressures in*
683 *the central North Sea: Implications for trap integrity and drilling safety*. Paper presented at
684 Geological Society, London, Petroleum Geology Conference series. 4(1), 1305-1313.
685 <https://doi.org/10.1144/0041305>
- 686 Gangi, A. F., & Carlson, R. L. (1996). An asperity-deformation model for effective pressure.
687 *Tectonophysics*, 256, 241–251. [https://doi.org/10.1016/0040-1951\(95\)00167-0](https://doi.org/10.1016/0040-1951(95)00167-0)
- 688 Ghabezloo, S., Sulem, J., Guedon, S., & Martineau, F. (2009). Effective stress law for the
689 permeability of a limestone. *International Journal of Rock Mechanics and Mining Sciences*,
690 46(2), 297-306. <https://doi.org/10.1016/j.ijrmms.2008.05.006>
- 691 Ingraham, M. D., Bauer, S. J., Issenm K. A., & Dewers, T. A. (2017). Evolution of permeability and
692 Biot coefficient at high mean stresses in high porosity sandstone. *International Journal of*
693 *Rock Mechanics & Mining Sciences*, 96, 1–10. <https://doi.org/10.1016/j.ijrmms.2017.04.004>
- 694 Jaeger, J. C., & Cook N. G. W. (1979). *Fundamentals of Rock Mechanics*, Chapman and Hall, New
695 York.
- 696 Li, M., Bernabé, Y., Xiao, W. L., Chen, Z. Y., & Liu, Z. Q. (2009). Effective pressure law for
697 permeability of E-bei sandstones. *Journal of Geophysical Research*, 114(B07).
698 <https://doi.org/10.1029/2009JB006373>
- 699 Li, M., Xiao, W. L., Bernabé, Y., & Zhao, J. Z. (2014). Nonlinear effective pressure law for
700 permeability. *Journal of Geophysical Research: Solid Earth*, 119, 302-318.
701 <https://doi.org/10.1002/2013JB010485>

- 702 Li, X., Wei, H., Chen, B., Liu, X., Wang, W., & Zhao, X. (2008). *Multi-stage fracturing stimulations*
703 *improve well performance in tight oil resevoirs of the Changqing Oilfield*. Paper presented at
704 International Petroleum Technology Conference, Kuala Lumpur, Malaysia.
705 <https://doi.org/10.2523/IPTC-12303-MS>
- 706 Mondol, N. H., Jahren, J., Bjørlykke, K., & Brevik, I. (2008). Elastic properties of clay minerals. *The*
707 *Leading Edge*, 27(6), 758-770. <https://doi.org/10.1190/1.2944161>
- 708 Robin, P. Y. (1973). Note on effective pressure. *Journal of Geophysical Research*, 78, 2434–2437.
709 <https://doi.org/10.1029/JB078i014p02434>
- 710 Siggins, A. F. & Dewhurst, D. N. (2003). Saturation, pore pressure and effective stress from
711 sandstone acoustic properties. *Geophysical Research Letters*, 30(2).
712 <https://doi.org/10.1029/2002GL016143>
- 713 Sokolnikoff, I. S. (1956). *Mathematical Theory of Elasticity*, McGraw-Hill, New York.
- 714 Terzaghi, K. (1943). *Theoretical Soil Mechanics*, John Wiley, New York.
- 715 Todd, T., & Simmons, G. (1972). Effect of pore pressure on the velocity of compressional waves in
716 low-porosity rocks. *Journal of Geophysical Research*, 77(20), 3731-3743.
717 <https://doi.org/10.1029/JB077i020p03731>
- 718 Walls, J., & Nur, A. (1979). *Pore pressure and confining pressure dependence of permeability in*
719 *sandstone*. Paper presented at the 7th Formation Evaluation Symposium of the Canadian Well
720 Logging Society.
- 721 Zoback, M. D., & Byerlee, J. D. (1975). Permeability and effective stress. *AAPG Bulletin*, 59(1),
722 154-158. <https://doi.org/10.1306/83D91C40-16C7-11D7-8645000102C1865D>

Table S2. All data of stress dependent effective stress coefficient in this research. Poisson's ratio of clay and grains $\nu = 0.25$, the shear modulus of grains $\mu_g=23.2\text{GPa}$.

¹Effective stress coefficient denoted as α .

²Clay fraction (F_c) defined by Eq. (2) in main text.

³Porosity denoted as ϕ .

Confining stress (MPa)	Pore pressure (MPa)	¹ α	α	α	α	α	α	α
		[² $F_c=0.3$, ³ $\phi=0.2$, Clay1]	[$F_c =0.3$, $\phi=0.1$, Clay1]	[$F_c =0.05$, $\phi=0.2$, Clay3]	[$F_c =0.3$, $\phi=0.2$, Clay2]	[$F_c =0.3$, $\phi=0.2$, Clay3]	[$F_c =0.1$, $\phi=0.2$, Clay1]	[$F_c =0.2$, $\phi=0.2$, Clay1]
2	2	3.282	4.540	0.979	1.903	1.434	2.407	3.060
4	2	3.257	4.508	0.978	1.884	1.422	2.395	3.041
6	2	3.233	4.476	0.977	1.866	1.411	2.383	3.023
8	2	3.211	4.445	0.976	1.850	1.401	2.373	3.007
10	2	3.190	4.415	0.975	1.836	1.392	2.363	2.991
12	2	3.171	4.385	0.974	1.823	1.384	2.354	2.977
14	2	3.152	4.356	0.973	1.811	1.377	2.347	2.964
16	2	3.136	4.328	0.972	1.801	1.371	2.340	2.952
18	2	3.121	4.301	0.972	1.793	1.366	2.334	2.941
20	2	3.107	4.275	0.971	1.786	1.362	2.328	2.931
22	2	3.095	4.249	0.970	1.781	1.358	2.324	2.922
24	2	3.084	4.225	0.970	1.778	1.356	2.321	2.915
26	2	3.074	4.202	0.969	1.776	1.354	2.318	2.908
28	2	3.066	4.180	0.969	1.775	1.354	2.316	2.903
30	2	3.060	4.159	0.968	1.777	1.354	2.315	2.899

32	2	3.055	4.139	0.968	1.780	1.356	2.315	2.896
34	2	3.051	4.121	0.968	1.784	1.358	2.316	2.894
36	2	3.049	4.103	0.967	1.790	1.361	2.318	2.893
38	2	3.049	4.088	0.967	1.798	1.366	2.320	2.894
40	2	3.050	4.073	0.967	1.807	1.371	2.323	2.895
42	2	3.052	4.060	0.967	1.818	1.377	2.328	2.898
44	2	3.056	4.049	0.967	1.831	1.384	2.333	2.902
46	2	3.062	4.039	0.967	1.845	1.392	2.339	2.907
48	2	3.069	4.030	0.967	1.861	1.401	2.345	2.913
50	2	3.078	4.024	0.968	1.878	1.410	2.353	2.920
4	4	2.739	3.802	0.976	1.779	1.390	2.036	2.561
6	4	2.725	3.778	0.975	1.770	1.382	2.029	2.551
8	4	2.712	3.755	0.974	1.761	1.375	2.024	2.541
10	4	2.699	3.732	0.973	1.753	1.368	2.019	2.533
12	4	2.688	3.710	0.972	1.746	1.361	2.014	2.525
14	4	2.677	3.688	0.971	1.740	1.356	2.010	2.517
16	4	2.667	3.667	0.971	1.735	1.351	2.006	2.510
18	4	2.658	3.647	0.970	1.731	1.347	2.003	2.503
20	4	2.649	3.627	0.969	1.727	1.344	2.000	2.497
22	4	2.642	3.608	0.969	1.724	1.341	1.998	2.492
24	4	2.635	3.590	0.968	1.722	1.339	1.996	2.488
26	4	2.629	3.573	0.967	1.721	1.338	1.995	2.484
28	4	2.624	3.556	0.967	1.720	1.337	1.994	2.480

30	4	2.619	3.540	0.967	1.721	1.337	1.993	2.477
32	4	2.616	3.526	0.966	1.722	1.338	1.993	2.475
34	4	2.613	3.512	0.966	1.724	1.339	1.993	2.474
36	4	2.612	3.499	0.966	1.727	1.342	1.993	2.473
38	4	2.611	3.486	0.966	1.731	1.344	1.994	2.472
40	4	2.611	3.475	0.966	1.735	1.348	1.996	2.473
42	4	2.611	3.465	0.965	1.741	1.352	1.998	2.473
44	4	2.613	3.456	0.965	1.747	1.357	2.000	2.475
46	4	2.615	3.447	0.966	1.754	1.363	2.003	2.477
48	4	2.619	3.440	0.966	1.762	1.369	2.007	2.479
50	4	2.623	3.434	0.966	1.771	1.376	2.010	2.483
6	6	2.395	3.307	0.974	1.696	1.361	1.808	2.246
8	6	2.386	3.288	0.972	1.690	1.356	1.803	2.240
10	6	2.378	3.270	0.972	1.685	1.351	1.800	2.234
12	6	2.370	3.253	0.971	1.680	1.346	1.797	2.229
14	6	2.363	3.235	0.970	1.676	1.342	1.794	2.224
16	6	2.356	3.219	0.969	1.673	1.339	1.792	2.219
18	6	2.350	3.203	0.968	1.670	1.336	1.790	2.215
20	6	2.344	3.188	0.968	1.667	1.333	1.788	2.211
22	6	2.339	3.173	0.967	1.665	1.331	1.787	2.207
24	6	2.335	3.159	0.966	1.664	1.329	1.786	2.204
26	6	2.331	3.146	0.966	1.663	1.328	1.785	2.202
28	6	2.328	3.133	0.965	1.663	1.327	1.784	2.200

30	6	2.325	3.121	0.965	1.663	1.327	1.784	2.198
32	6	2.323	3.110	0.965	1.664	1.327	1.784	2.197
34	6	2.322	3.099	0.964	1.665	1.328	1.784	2.196
36	6	2.321	3.089	0.964	1.667	1.329	1.785	2.196
38	6	2.321	3.080	0.964	1.670	1.331	1.786	2.196
40	6	2.321	3.072	0.964	1.673	1.333	1.787	2.196
42	6	2.322	3.064	0.964	1.677	1.335	1.788	2.197
44	6	2.324	3.057	0.964	1.681	1.339	1.790	2.198
46	6	2.326	3.051	0.964	1.686	1.342	1.792	2.200
48	6	2.329	3.046	0.964	1.691	1.346	1.795	2.202
50	6	2.333	3.042	0.964	1.697	1.350	1.797	2.204
8	8	2.156	2.950	0.971	1.631	1.344	1.650	2.028
10	8	2.150	2.935	0.970	1.627	1.340	1.648	2.024
12	8	2.144	2.920	0.969	1.623	1.336	1.646	2.020
14	8	2.139	2.907	0.968	1.620	1.333	1.644	2.017
16	8	2.134	2.893	0.967	1.618	1.330	1.643	2.013
18	8	2.130	2.881	0.967	1.615	1.328	1.642	2.011
20	8	2.127	2.869	0.966	1.614	1.325	1.640	2.008
22	8	2.123	2.857	0.965	1.612	1.324	1.640	2.006
24	8	2.121	2.846	0.965	1.611	1.322	1.639	2.004
26	8	2.118	2.835	0.964	1.611	1.321	1.638	2.003
28	8	2.116	2.825	0.964	1.611	1.320	1.638	2.001
30	8	2.115	2.816	0.963	1.611	1.320	1.638	2.000

32	8	2.114	2.808	0.963	1.612	1.320	1.639	2.000
34	8	2.114	2.799	0.963	1.613	1.320	1.639	2.000
36	8	2.114	2.792	0.962	1.615	1.321	1.640	2.000
38	8	2.114	2.785	0.962	1.617	1.322	1.640	2.000
40	8	2.116	2.779	0.962	1.619	1.323	1.641	2.001
42	8	2.117	2.774	0.962	1.622	1.325	1.643	2.002
44	8	2.119	2.769	0.962	1.625	1.327	1.644	2.003
46	8	2.121	2.765	0.962	1.629	1.329	1.646	2.005
48	8	2.124	2.761	0.962	1.633	1.332	1.648	2.007
50	8	2.128	2.758	0.963	1.638	1.335	1.650	2.009
10	10	1.979	2.680	0.968	1.576	1.331	1.537	1.868
12	10	1.975	2.668	0.967	1.574	1.327	1.535	1.866
14	10	1.972	2.656	0.966	1.571	1.325	1.534	1.863
16	10	1.969	2.646	0.966	1.569	1.322	1.533	1.861
18	10	1.966	2.635	0.965	1.568	1.320	1.532	1.859
20	10	1.963	2.626	0.964	1.566	1.318	1.532	1.857
22	10	1.961	2.616	0.964	1.565	1.316	1.531	1.856
24	10	1.960	2.607	0.963	1.565	1.315	1.531	1.855
26	10	1.959	2.599	0.963	1.564	1.314	1.531	1.854
28	10	1.958	2.591	0.962	1.564	1.313	1.531	1.854
30	10	1.957	2.584	0.962	1.565	1.313	1.531	1.853
32	10	1.957	2.577	0.961	1.565	1.313	1.531	1.853
34	10	1.958	2.571	0.961	1.566	1.313	1.532	1.853

36	10	1.958	2.566	0.961	1.568	1.313	1.533	1.854
38	10	1.959	2.561	0.961	1.570	1.314	1.534	1.855
40	10	1.961	2.556	0.961	1.572	1.314	1.535	1.856
42	10	1.963	2.552	0.961	1.574	1.316	1.536	1.857
44	10	1.965	2.549	0.961	1.577	1.317	1.537	1.859
46	10	1.968	2.546	0.961	1.580	1.319	1.539	1.860
48	10	1.971	2.544	0.961	1.584	1.321	1.541	1.863
50	10	1.974	2.542	0.961	1.587	1.323	1.543	1.865
12	12	1.844	2.469	0.966	1.530	1.319	1.451	1.746
14	12	1.842	2.459	0.965	1.528	1.317	1.450	1.745
16	12	1.840	2.450	0.964	1.527	1.315	1.449	1.743
18	12	1.838	2.442	0.963	1.525	1.313	1.449	1.742
20	12	1.836	2.434	0.963	1.524	1.311	1.448	1.741
22	12	1.835	2.427	0.962	1.524	1.309	1.448	1.740
24	12	1.835	2.420	0.961	1.523	1.308	1.448	1.740
26	12	1.834	2.413	0.961	1.523	1.307	1.448	1.739
28	12	1.834	2.407	0.960	1.523	1.306	1.448	1.739
30	12	1.834	2.401	0.960	1.524	1.306	1.449	1.739
32	12	1.835	2.396	0.960	1.524	1.305	1.449	1.740
34	12	1.836	2.391	0.959	1.525	1.305	1.450	1.740
36	12	1.837	2.387	0.959	1.527	1.306	1.451	1.741
38	12	1.838	2.383	0.959	1.528	1.306	1.452	1.742
40	12	1.840	2.380	0.959	1.530	1.307	1.453	1.744

42	12	1.843	2.378	0.959	1.532	1.307	1.454	1.745
44	12	1.845	2.375	0.959	1.535	1.308	1.455	1.747
46	12	1.848	2.374	0.959	1.538	1.310	1.457	1.749
48	12	1.851	2.373	0.959	1.541	1.311	1.458	1.751
50	12	1.855	2.372	0.959	1.544	1.313	1.460	1.753
14	14	1.738	2.300	0.963	1.490	1.310	1.384	1.651
16	14	1.737	2.293	0.962	1.489	1.308	1.383	1.650
18	14	1.736	2.286	0.962	1.488	1.306	1.383	1.649
20	14	1.735	2.279	0.961	1.487	1.304	1.383	1.648
22	14	1.734	2.273	0.960	1.487	1.303	1.383	1.648
24	14	1.734	2.268	0.960	1.486	1.302	1.383	1.648
26	14	1.734	2.262	0.959	1.486	1.301	1.383	1.648
28	14	1.735	2.258	0.959	1.487	1.300	1.383	1.648
30	14	1.736	2.253	0.958	1.487	1.299	1.384	1.649
32	14	1.737	2.249	0.958	1.488	1.299	1.384	1.650
34	14	1.738	2.246	0.958	1.489	1.299	1.385	1.650
36	14	1.740	2.243	0.958	1.490	1.299	1.386	1.651
38	14	1.741	2.240	0.957	1.492	1.299	1.387	1.653
40	14	1.744	2.238	0.957	1.494	1.299	1.388	1.654
42	14	1.746	2.236	0.957	1.496	1.300	1.389	1.656
44	14	1.749	2.235	0.957	1.498	1.301	1.391	1.658
46	14	1.752	2.234	0.957	1.500	1.302	1.392	1.660
48	14	1.755	2.234	0.957	1.503	1.303	1.394	1.662

50	14	1.759	2.234	0.958	1.506	1.304	1.395	1.664
16	16	1.652	2.162	0.961	1.455	1.301	1.330	1.574
18	16	1.652	2.157	0.960	1.455	1.299	1.330	1.573
20	16	1.652	2.151	0.959	1.454	1.298	1.330	1.573
22	16	1.652	2.147	0.959	1.454	1.296	1.330	1.573
24	16	1.652	2.142	0.958	1.454	1.295	1.330	1.573
26	16	1.653	2.138	0.958	1.454	1.294	1.330	1.574
28	16	1.654	2.134	0.957	1.454	1.293	1.331	1.574
30	16	1.655	2.131	0.957	1.455	1.293	1.331	1.575
32	16	1.656	2.128	0.956	1.455	1.292	1.332	1.576
34	16	1.658	2.125	0.956	1.456	1.292	1.333	1.577
36	16	1.660	2.123	0.956	1.458	1.292	1.334	1.578
38	16	1.662	2.121	0.956	1.459	1.292	1.335	1.580
40	16	1.664	2.120	0.956	1.461	1.292	1.336	1.581
42	16	1.667	2.119	0.956	1.463	1.293	1.337	1.583
44	16	1.670	2.119	0.956	1.465	1.293	1.338	1.585
46	16	1.673	2.119	0.956	1.467	1.294	1.340	1.587
48	16	1.676	2.119	0.956	1.470	1.295	1.341	1.589
50	16	1.680	2.120	0.956	1.472	1.296	1.343	1.592
18	18	1.582	2.049	0.958	1.425	1.293	1.286	1.511
20	18	1.583	2.044	0.958	1.425	1.292	1.286	1.511
22	18	1.583	2.040	0.957	1.424	1.290	1.286	1.511
24	18	1.584	2.037	0.956	1.424	1.289	1.287	1.512

26	18	1.585	2.033	0.956	1.425	1.288	1.287	1.512
28	18	1.586	2.031	0.955	1.425	1.288	1.288	1.513
30	18	1.587	2.028	0.955	1.426	1.287	1.288	1.514
32	18	1.589	2.026	0.955	1.426	1.286	1.289	1.515
34	18	1.591	2.024	0.954	1.427	1.286	1.290	1.516
36	18	1.593	2.023	0.954	1.429	1.286	1.291	1.518
38	18	1.595	2.022	0.954	1.430	1.286	1.292	1.519
40	18	1.598	2.021	0.954	1.432	1.286	1.293	1.521
42	18	1.601	2.021	0.954	1.433	1.286	1.294	1.523
44	18	1.604	2.021	0.954	1.435	1.287	1.295	1.525
46	18	1.607	2.021	0.954	1.438	1.287	1.297	1.527
48	18	1.610	2.022	0.954	1.440	1.288	1.298	1.529
50	18	1.614	2.023	0.954	1.443	1.289	1.300	1.532
20	20	1.524	1.953	0.956	1.398	1.286	1.250	1.459
22	20	1.525	1.950	0.955	1.398	1.285	1.250	1.459
24	20	1.526	1.947	0.955	1.398	1.284	1.250	1.460
26	20	1.527	1.945	0.954	1.398	1.283	1.251	1.461
28	20	1.529	1.942	0.954	1.399	1.282	1.251	1.462
30	20	1.530	1.941	0.953	1.399	1.281	1.252	1.463
32	20	1.532	1.939	0.953	1.400	1.281	1.253	1.464
34	20	1.534	1.938	0.953	1.401	1.281	1.254	1.465
36	20	1.537	1.937	0.953	1.403	1.280	1.255	1.467
38	20	1.539	1.937	0.952	1.404	1.280	1.256	1.468

40	20	1.542	1.937	0.952	1.405	1.280	1.257	1.470
42	20	1.545	1.937	0.952	1.407	1.280	1.258	1.472
44	20	1.548	1.937	0.952	1.409	1.281	1.259	1.474
46	20	1.551	1.938	0.952	1.411	1.281	1.261	1.476
48	20	1.554	1.939	0.952	1.413	1.282	1.262	1.479
50	20	1.558	1.941	0.953	1.416	1.282	1.264	1.481
22	22	1.475	1.872	0.954	1.374	1.280	1.219	1.415
24	22	1.477	1.870	0.953	1.374	1.279	1.220	1.416
26	22	1.478	1.868	0.953	1.375	1.278	1.220	1.417
28	22	1.480	1.867	0.952	1.375	1.277	1.221	1.418
30	22	1.481	1.865	0.952	1.376	1.276	1.222	1.419
32	22	1.484	1.864	0.951	1.377	1.276	1.222	1.420
34	22	1.486	1.864	0.951	1.378	1.275	1.223	1.422
36	22	1.488	1.863	0.951	1.379	1.275	1.224	1.423
38	22	1.491	1.863	0.951	1.380	1.275	1.225	1.425
40	22	1.494	1.864	0.951	1.382	1.275	1.226	1.427
42	22	1.496	1.864	0.951	1.384	1.275	1.228	1.429
44	22	1.500	1.865	0.951	1.385	1.275	1.229	1.431
46	22	1.503	1.867	0.951	1.387	1.275	1.230	1.433
48	22	1.506	1.868	0.951	1.390	1.276	1.232	1.435
50	22	1.510	1.870	0.951	1.392	1.276	1.233	1.438
24	24	1.434	1.803	0.951	1.353	1.274	1.194	1.378
26	24	1.436	1.802	0.951	1.354	1.273	1.194	1.379

28	24	1.437	1.801	0.950	1.354	1.272	1.195	1.381
30	24	1.439	1.800	0.950	1.355	1.271	1.196	1.382
32	24	1.441	1.800	0.950	1.356	1.271	1.197	1.383
34	24	1.444	1.799	0.949	1.357	1.270	1.197	1.385
36	24	1.446	1.799	0.949	1.358	1.270	1.198	1.386
38	24	1.449	1.800	0.949	1.359	1.270	1.199	1.388
40	24	1.452	1.800	0.949	1.361	1.270	1.200	1.390
42	24	1.455	1.801	0.949	1.362	1.270	1.202	1.392
44	24	1.458	1.803	0.949	1.364	1.270	1.203	1.394
46	24	1.461	1.804	0.949	1.366	1.270	1.204	1.396
48	24	1.465	1.806	0.949	1.368	1.271	1.205	1.398
50	24	1.468	1.808	0.949	1.370	1.271	1.207	1.401
26	26	1.399	1.744	0.949	1.334	1.268	1.172	1.347
28	26	1.401	1.743	0.949	1.335	1.268	1.173	1.348
30	26	1.403	1.743	0.949	1.336	1.267	1.174	1.349
32	26	1.405	1.743	0.948	1.337	1.266	1.174	1.351
34	26	1.407	1.743	0.948	1.338	1.266	1.175	1.352
36	26	1.410	1.743	0.948	1.339	1.266	1.176	1.354
38	26	1.413	1.744	0.948	1.340	1.265	1.177	1.356
40	26	1.415	1.745	0.947	1.342	1.265	1.178	1.358
42	26	1.418	1.746	0.947	1.343	1.265	1.179	1.360
44	26	1.422	1.748	0.947	1.345	1.265	1.180	1.362
46	26	1.425	1.750	0.947	1.347	1.265	1.182	1.364

48	26	1.428	1.752	0.947	1.349	1.266	1.183	1.366
50	26	1.432	1.754	0.948	1.351	1.266	1.184	1.368
28	28	1.368	1.692	0.948	1.318	1.264	1.154	1.320
30	28	1.371	1.692	0.947	1.319	1.263	1.154	1.321
32	28	1.373	1.693	0.947	1.319	1.262	1.155	1.323
34	28	1.375	1.693	0.947	1.320	1.262	1.156	1.324
36	28	1.378	1.694	0.946	1.322	1.261	1.157	1.326
38	28	1.381	1.695	0.946	1.323	1.261	1.158	1.328
40	28	1.384	1.696	0.946	1.324	1.261	1.159	1.330
42	28	1.387	1.698	0.946	1.326	1.261	1.160	1.331
44	28	1.390	1.699	0.946	1.327	1.261	1.161	1.334
46	28	1.393	1.701	0.946	1.329	1.261	1.162	1.336
48	28	1.397	1.703	0.946	1.331	1.261	1.164	1.338
50	28	1.400	1.706	0.946	1.333	1.261	1.165	1.340
30	30	1.342	1.648	0.946	1.303	1.259	1.138	1.297
32	30	1.345	1.648	0.946	1.304	1.258	1.139	1.298
34	30	1.347	1.649	0.945	1.305	1.258	1.139	1.300
36	30	1.350	1.650	0.945	1.306	1.257	1.140	1.302
38	30	1.353	1.651	0.945	1.307	1.257	1.141	1.303
40	30	1.355	1.653	0.945	1.309	1.257	1.142	1.305
42	30	1.358	1.654	0.945	1.310	1.257	1.143	1.307
44	30	1.362	1.656	0.945	1.312	1.257	1.144	1.309
46	30	1.365	1.658	0.945	1.313	1.257	1.146	1.311

48	30	1.368	1.661	0.945	1.315	1.257	1.147	1.313
50	30	1.372	1.663	0.945	1.317	1.257	1.148	1.316
32	32	1.320	1.609	0.945	1.290	1.255	1.124	1.277
34	32	1.322	1.610	0.944	1.291	1.254	1.125	1.278
36	32	1.325	1.611	0.944	1.292	1.254	1.126	1.280
38	32	1.328	1.613	0.944	1.293	1.254	1.127	1.282
40	32	1.331	1.614	0.944	1.294	1.253	1.128	1.284
42	32	1.334	1.616	0.943	1.296	1.253	1.129	1.285
44	32	1.337	1.618	0.943	1.297	1.253	1.130	1.288
46	32	1.340	1.620	0.943	1.299	1.253	1.131	1.290
48	32	1.343	1.623	0.943	1.301	1.253	1.132	1.292
50	32	1.347	1.626	0.943	1.303	1.253	1.133	1.294
34	34	1.300	1.575	0.943	1.278	1.251	1.112	1.259
36	34	1.303	1.576	0.943	1.279	1.251	1.113	1.261
38	34	1.306	1.578	0.943	1.280	1.250	1.114	1.263
40	34	1.309	1.580	0.943	1.282	1.250	1.115	1.265
42	34	1.312	1.582	0.942	1.283	1.250	1.116	1.267
44	34	1.315	1.584	0.942	1.285	1.250	1.117	1.269
46	34	1.318	1.586	0.942	1.286	1.250	1.118	1.271
48	34	1.321	1.589	0.942	1.288	1.250	1.120	1.273
50	34	1.325	1.592	0.942	1.290	1.250	1.121	1.275
36	36	1.283	1.545	0.942	1.268	1.248	1.103	1.245
38	36	1.286	1.547	0.942	1.269	1.247	1.103	1.246

40	36	1.289	1.549	0.942	1.270	1.247	1.104	1.248
42	36	1.292	1.551	0.942	1.272	1.247	1.105	1.250
44	36	1.295	1.553	0.941	1.273	1.247	1.106	1.252
46	36	1.298	1.556	0.941	1.275	1.247	1.107	1.254
48	36	1.302	1.558	0.941	1.276	1.247	1.109	1.256
50	36	1.305	1.561	0.941	1.278	1.247	1.110	1.258
38	38	1.269	1.519	0.941	1.259	1.245	1.094	1.232
40	38	1.272	1.521	0.941	1.260	1.244	1.095	1.234
42	38	1.275	1.524	0.941	1.261	1.244	1.096	1.236
44	38	1.278	1.526	0.941	1.263	1.244	1.097	1.238
46	38	1.281	1.528	0.941	1.264	1.244	1.098	1.240
48	38	1.284	1.531	0.940	1.266	1.244	1.099	1.242
50	38	1.287	1.534	0.940	1.268	1.244	1.100	1.244
40	40	1.257	1.497	0.941	1.251	1.242	1.087	1.221
42	40	1.259	1.499	0.940	1.252	1.242	1.088	1.223
44	40	1.262	1.501	0.940	1.254	1.242	1.089	1.225
46	40	1.265	1.504	0.940	1.255	1.241	1.090	1.227
48	40	1.269	1.507	0.940	1.257	1.241	1.091	1.229
50	40	1.272	1.510	0.940	1.258	1.241	1.092	1.231
42	42	1.246	1.477	0.940	1.244	1.240	1.081	1.212
44	42	1.249	1.479	0.940	1.245	1.240	1.082	1.214
46	42	1.252	1.482	0.939	1.247	1.239	1.083	1.216
48	42	1.255	1.485	0.939	1.248	1.239	1.084	1.218

50	42	1.258	1.488	0.939	1.250	1.239	1.085	1.220
44	44	1.237	1.460	0.939	1.238	1.238	1.076	1.204
46	44	1.240	1.463	0.939	1.240	1.238	1.077	1.206
48	44	1.243	1.465	0.939	1.241	1.237	1.078	1.208
50	44	1.246	1.468	0.939	1.243	1.237	1.079	1.210
46	46	1.230	1.445	0.939	1.233	1.236	1.073	1.198
48	46	1.233	1.448	0.939	1.235	1.236	1.074	1.200
50	46	1.236	1.451	0.939	1.236	1.236	1.075	1.202
48	48	1.224	1.433	0.939	1.229	1.235	1.070	1.193
50	48	1.227	1.436	0.938	1.231	1.234	1.071	1.195
50	50	1.219	1.422	0.938	1.226	1.233	1.068	1.190
